Germline deletion of *Cetn1* causes infertility in male mice

Prachee Avasthi[1,*,‡], Jan Frederik Scheel[2,‡], Guoxin Ying[1], Jeanne M. Frederick[1], Wolfgang Baehr[1,3,4,§] and Uwe Wolfrum[2,§]

[1]Department of Ophthalmology, University of Utah Health Science Center, 65 Mario Capecchi Drive, Salt Lake City, UT 84132, USA
[2]Department of Cell and Matrix Biology, Institute of Zoology, Johannes Gutenberg University Mainz, D-55099 Mainz, Germany
[3]Department of Biology, University of Utah, 257 South 1400 East, Salt Lake City, Utah 84112, USA
[4]Department of Neurobiology and Anatomy, University of Utah Health Science Center, 20 N. Medical Drive, Room 401, Salt Lake City, UT 84132, USA

*Present address: Departments of Biochemistry and Biophysics, University of California, San Francisco, CA 94158, USA
‡These authors contributed equally to this work
§Authors for correspondence (wbaehr@hsc.utah.edu; wolfrum@uni-mainz.de)

Accepted 10 April 2013
Journal of Cell Science 126, 3204–3213

doi: 10.1242/jcs.128587

Summary

Centrins are calmodulin-like Ca^{2+}-binding proteins that can be found in all ciliated eukaryotic cells from yeast to mammals. Expressed in male germ cells and photoreceptors, centrin 1 (CETN1) resides in the photoreceptor transition zone and connecting cilium. To identify its function in mammals, we deleted *Cetn1* by homologous recombination. *Cetn1*$^{-/-}$ mice were viable and showed no sign of retina degeneration suggesting that CETN1 is nonessential for photoreceptor ciliogenesis or structural maintenance. Phototransduction components localized normally to the *Cetn1*$^{-/-}$ photoreceptor outer segments, and loss of CETN1 had no effect on light-induced translocation of transducin to the inner segment. Although *Cetn1*$^{-/-}$ females and *Cetn1*$^{+/-}$ males had normal fertility, *Cetn1*$^{-/-}$ males were infertile. The *Cetn1*$^{-/-}$ testes size was normal, and spermatogonia as well as spermatocytes developed normally. However, spermatids lacked tails suggesting severe defects at the late maturation phase of spermiogenesis. Viable sperm cells were absent and the few surviving spermatozoa were malformed. Light and electron microscopy analyses of *Cetn1*$^{-/-}$ spermatids revealed failures in centriole rearrangement during basal body maturation and in the basal-body–nucleus connection. These results confirm an essential role for CETN1 in late steps of spermiogenesis and spermatid maturation.

Key words: Centrin, CETN1 deletion, Photoreceptors, Spermiogenesis, Spermatid maturation, Flagella

Introduction

Centrins ('caltractins') are small, acidic proteins belonging to the Ca^{2+}-binding EF-hand protein family (50% identity with calmodulin). As eukaryotic signature proteins, they are found in all eukaryotic cells from unicellular organisms (Zhang and He, 2012) to mammals (Wolfrum et al., 2002). Centrins commonly associate with centrioles of centrosomes and centrosomal-related structures, i.e. basal bodies and spindle pole bodies (Geimer and Melkonian, 2005), but their function is largely unknown.

Rodents express four centrin isoforms (CETN1–4) encoded by four distinct genes (*Cetn1–4*), while the human genome contains only three isoforms (*CETN1–3*) (Friedberg, 2006). Sequences and domain structures of all centrin isoforms are highly conserved during evolution. Centrins, calmodulin and other Ca^{2+}-binding proteins of the parvalbumin superfamily with four EF-hand motifs derive from a common ancestor. Mammalian centrins diversified into two main branches containing CETN1, 2, 4 and CETN3 (Trojan et al., 2008). *CETN1* was cloned from a human testis expression library (Errabolu et al., 1994) and thought to be a retrotransposition of *CETN2* with typical characteristics of L1 retrotransposons and no consensus promoter element or Sp1 binding motifs (Hart et al., 1999). CETN1 is also expressed in rodent photoreceptors as well as other ciliated cells, including sperm (Giessl et al., 2004; Laoukili et al., 2000; Wolfrum and Salisbury, 1998). By contrast, CETN2 and CETN3 are expressed in all somatic cells where they are found associated with the centrosome and pericentriolar matrix (Gavet et al., 2003; Giessl et al., 2004; Laoukili et al., 2000; Salisbury et al., 2002). CETN2 is one of the first proteins acquired in newly formed centrioles during the cell cycle S-phase, and its knockdown in HeLa cells revealed abnormalities in spindle pole formation (Salisbury et al., 2002). However, CETN2 is not expressed in haploid male germ cells (Tanaka et al., 2010). Mammalian CETN3, thought to be involved in centrosome duplication, is closely related to the yeast centrin cdc31 (Middendorp et al., 1997; Middendorp et al., 2000). *Cetn4* was identified in the genome of rodents and was found expressed in ciliated cells and associated with daughter centrioles in photoreceptors (Gavet et al., 2003; Trojan et al., 2008).

The four mouse CETN isoforms are expressed differentially in the ciliary apparatus, the connecting cilium, the basal body and its adjacent centriole of photoreceptors (Giessl et al., 2004; Trojan et al., 2008; Wolfrum and Salisbury, 1998). CETN1 is expressed in basal body/connecting cilium (not in daughter centriole), CETN2,3 are expressed in basal body/connecting cilium and daughter centriole, while CETN4 is present only in daughter centrioles (Giessl et al., 2004). All centrins (CETN1–4) interact *in vitro* with the βγ subunits of the visual G protein

transducin (Tβγ) (Giessl et al., 2004; Pulvermüller et al., 2002). It was predicted that CETN1 and CETN2 regulate transducin translocation between photoreceptor outer and inner segments (Giessl et al., 2006), a pathway that plays an important role light-adaptation and desensitization (Sokolov et al., 2002).

A critical role for CETN1 in testis was hypothesized due to its prominent expression in the tissue (Hart et al., 1999). The testis harbors the reproductive epithelia, the tubuli seminiferi, and facilitates the constant production of spermatids from spermatogonia during the process of spermatogenesis. In mice, spermatogenesis is accomplished in four rounds of cycles divided into twelve morphological stages of the seminifereous tubules, specified by capital Roman numerals (I–XII) (Oakberg, 1956). Germ cell maturation in seminifereous tubules takes 35 days in mouse and the process is divided into three main phases: mitotic division of the spermatogonia, meiosis of spermatocytes into four haploid spermatids and morphogenesis into mature spermatozoa. These maturation events are termed collectively spermiogenesis (reviewed by Cooke and Saunders, 2002). The sixteen steps of spermatid development are specified with Arabic numbers (1–16) (Oakberg, 1956). Previous studies described CETN1 localization as restricted to the outermost layer of seminifereous tubules colocalizing with SUMO2/3 (Klein and Nigg, 2009; Tanaka et al., 2010).

While the functions of CETN2 in centriole genesis, DNA repair and mRNA export have been investigated over the last decade, little is known of CETN1 function (reviewed in: Dantas et al., 2012; Trojan et al., 2008). We generated floxed *Cetn1* mice and deleted the single coding exon to generate global knockouts. In germline deletions of *Cetn1*, we were unable to observe defects in light-induced translocation of transducin, likely due to redundancy with other centrins. Male germline $Cetn1^{-/-}$ mice, however, were infertile suggesting defects in sperm development. Microscopic analysis showed that $Cetn1^{-/-}$ sperm heads were often abnormally shaped, midpieces and principle pieces of tails were reduced in length or absent. These results are consistent with an essential role for CETN1 in spermiogenesis and maturation.

Results

Photoreceptor and germline deletion of the *Cetn1* gene

The mouse *Cetn1* gene consists of a coding exon 1 and a noncoding 3′-UTR exon 2 (Fig. 1A). Presence of an intron suggests that the *Cetn1* gene may not be an expressed retrotransposon (Hart et al., 1999). Our construct permitted deletions of the coding exon and the neo cassette in intron 1 (Fig. 1B,C). After blastocyst injection of the 3*loxP* construct, three chimeras were born and outcrossed to produce F1 heterozygotes. By PCR analysis, all F1 heterozygotes contained one wild-type allele and one 3*loxP*-containing correctly targeted allele (Fig. 1B). We followed a strategy to first generate rod-specific deletions to avoid embryonic lethality, followed by germline deletions to monitor non-retina phenotypes. For deletions in rods, homozygous 3*loxP*;*iCre75* mice were generated by expressing Cre recombinase driven by the mouse opsin promoter (Avasthi et al., 2009; Li et al., 2005). Germline deletion was achieved by mating 3*loxP* mice with a mosaic *Cre* line which expresses Cre recombinase under the control of the adenovirus *EIIa* promoter in mouse embryos. We selected offspring with high relative amount of full *Cetn1* locus deletion by semi-quantitative PCR, and outcrossed these to generate

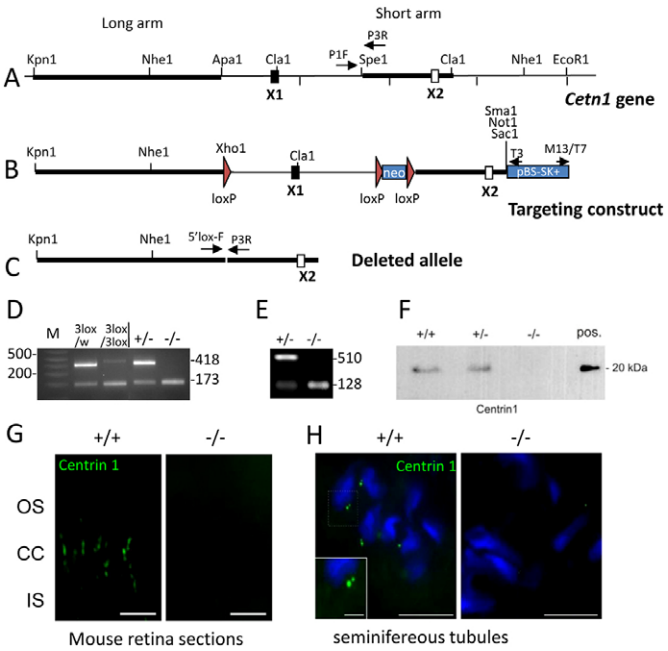

Fig. 1. *Cetn1* deletion. (**A**) The endogenous *Cetn1* locus with one coding exon (X1) and one non-coding exon (X2). Long arm, short arm, *loxP* sites (red triangles) and relevant enzyme restriction sites are indicated. (**B**) The 3*loxP* knock-in construct with *loxP* sites flanking exon1 and neo for eventual deletion. (**C**) The deleted *Cetn1* gene. (**D**) Genotyping of $Cetn1^{loxP/WT}$;$iCre75^{+}$ (labeled 3lox/w) and of $Cetn1^{3loxP/3loxP}$;$iCre75^{+}$ mice (labeled 3lox/3lox), and $Cetn1^{+/-}$ and $Cetn1^{-/-}$ mice with retina DNA as PCR template. PCR amplification detects a wild-type allele at 418 bp in $Cetn1^{+/-}$ and a deletion product at 173 bp in $Cetn1^{-/-}$ mice. (**E**) RT-PCR was performed on extracts from $Cetn1^{+/-}$ and $Cetn1^{-/-}$ testes; 510 bp amplicons were detected for $Cetn1^{+/-}$ but not for $Cetn1^{-/-}$. (**F**) Immunoblot of wild-type and $Cetn1^{-/-}$ testes protein extract. CETN1 is undetectable in the germline knockout mouse. (**G**) Immunohistochemistry of wild-type and $Cetn1^{-/-}$ retina cryosections using the anti-CETN1 antibody, MmC1. CETN1 localizes to wild-type photoreceptor cilia, but is undetectable in the $Cetn1^{-/-}$ retina. Scale bar: 10 µm. (**H**) CETN1 immunohistochemistry of wild-type seminifereous tubules. Antibody MmC1 detects characteristic dots (centrioles), one of which is brighter and bigger at the condensed nuclei in $Cetn1^{+/+}$tubules, whereas in $Cetn1^{-/-}$ tubules, labeling is undetectable. Scale bars: 10 µm; inset, 5 µm.

germline deletion mice (Holzenberger et al., 2000). $Cetn1^{+/-}$ mice and $Cetn1^{-/-}$ females were viable, normal sized and fertile, but $Cetn1^{-/-}$ males produced no offspring. No other phenotype was apparent in the knockout mice.

$Cetn1^{3lox/WT}$;$iCre75^{+}$, $Cetn1^{3lox/3lox}$;$iCre75^{+}$, $Cetn1^{+/-}$ and $Cetn1^{-/-}$ mice were tested for deletion of the *Cetn1* locus by PCR of retinal DNA. $Cetn1^{3lox/WT}$;$iCre75^{+}$ mice showed a wild-type allele product from primers P1F/P3R at 418 bp and the deletion allele product from primers 5′*loxF*/P3R at 173 bp (Fig. 1D). Global knockouts were also tested and contained wild-type and deleted products or deleted products alone for $Cetn1^{+/-}$ and $Cetn1^{-/-}$ mice, respectively (Fig. 1D). *Cetn1* deletion was further verified in testes where CETN1 is expressed abundantly (Hart et al., 1999). *Cetn1* mRNA transcripts were detected in $Cetn1^{+/+}$ and $Cetn1^{+/-}$ but were absent in $Cetn1^{-/-}$ testes (Fig. 1E). Immunoblot analyses of testes lysate with pre-adsorbed affinity-purified monospecific polyclonal MmC1 antibody revealed CETN1 expression in $Cetn1^{+/+}$ and $Cetn1^{+/-}$, but not in $Cetn1^{-/-}$ male mice (Fig. 1F). By

immunohistochemistry, CETN1 was undetectable in *Cetn1*$^{-/-}$ retina sections (Fig. 1G) and seminifereous tubules (Fig. 1H).

Phototransduction and light-dependent translocation of transducin are unaffected in *Cetn1*$^{-/-}$ mice

As part of desensitization and a neuroprotective mechanism, the photoreceptor heterotrimeric G protein, transducin, translocates to the rod inner segment in constant light (Sokolov et al., 2002). Light-activation of rhodopsin triggers GTP/GDP exchange on Tα causing Tα^{GTP} and Tβγ to dissociate and traffic to the inner segment in minutes (Calvert et al., 2006). We have shown that Ca^{2+}-activated centrin isoforms (CETN1,2,4) bind tightly to transducin via the Tβγ-subunits, and suggested that Ca^{2+}-dependent assemblies of centrin/G-protein complexes may regulate transducin movement through the connecting cilium (Giessl et al., 2006; Trojan et al., 2008). Immunohistochemistry using antibodies directed against rod Tα and Tγ showed no significant difference in light-induced translocation of transducin to the inner segments of *Cetn1*$^{+/+}$ and *Cetn1*$^{-/-}$ mice (Fig. 2A), suggesting that CETN1 is not absolutely required for translocation, or that its loss may be compensated by other centrin isoforms. Expression of CETN2, also localized to the photoreceptor connecting cilium, showed a 30% increase in *Cetn1*$^{-/-}$ retina mRNA (Fig. 2B) perhaps as compensation for CETN1 loss.

We examined *Cetn1*$^{-/-}$ retina sections for mislocalization of other rod and cone phototransduction proteins, including the most abundant proteins, the visual pigments rhodopsin and ML-opsin, as well as transducin (Tα, Tγ), PDE and channel subunits (CNGA1, CNGA3) (supplementary material Fig. S1). We observed no change in the distributions of these components in mature *Cetn1* knockout retinas relative to age-matched controls (supplementary material Fig. S1). Consistent with absence of retinal degeneration and correct localization of phototransduction components, *Cetn1*$^{-/-}$ animals showed no significant difference in scotopic ERG a-wave amplitudes in comparison to age-matched controls (Fig. 2C). Immunoblots revealed reduced levels of PDE6δ, the prenyl binding protein encoded by the Pde6d gene, as well as farnesylated GRK1 (rhodopsin kinase) (Fig. 2D).

Reproductive abnormalities of male *Cetn1*$^{-/-}$ mice

We next examined the cellular and molecular basis of *Cetn1*$^{-/-}$ male infertility by analyzing testes from six dedicated litters. *Cetn1*$^{-/-}$ testes mean size and weight were indistinguishable from those of control littermates (supplementary material Table S1). Quantification of cell number and thickness measurements of seminifereous tubule epithelia at spermatogenesis stage IX revealed no significant alteration in germ cell number or epithelial thickness (supplementary material Table S2; $n=5$). Light microscopy of semithin sections through the testes of *Cetn1*$^{-/-}$ mice showed normal morphologies of seminifereous tubules, Leydig cells and Sertoli cells except for missing mature spermatids with flagella (Fig. 3). Analyzing different spermatogenesis stages, we found all cell types characteristic of normal spermatogenesis in the outer and first layers of *Cetn1*$^{-/-}$ seminifereous epithelia. *Cetn1*$^{-/-}$spermatogonia, resting spermatocytes as well as spermatocytes in various phases of meiosis (supplementary material Fig. S2A–D), and round and elongating spermatids did not differ from *Cetn1*$^{+/+}$ males until step 12 of spermiogenesis. Ultrastructural examination provided no phenotypic difference in acrosome structure or structure of other organelles, e.g. the Golgi apparatus (supplementary material Fig. S3A–D). However, dense material of degraded spermatids was obvious in *Cetn1*$^{-/-}$ mice (Fig. 3, lower panels and supplementary material Fig. S2E,F), and mature-tailed spermatids anchored at the Sertoli cell ectoplasmic specialization as well as spermiated sperm were absent. In our extended ultrastructural analysis of seminifereous tubules we observed only one *Cetn1*$^{-/-}$ sperm flagellum in cross section showing apparent disorganization of axonemal microtubules (supplementary material Fig. S2H).

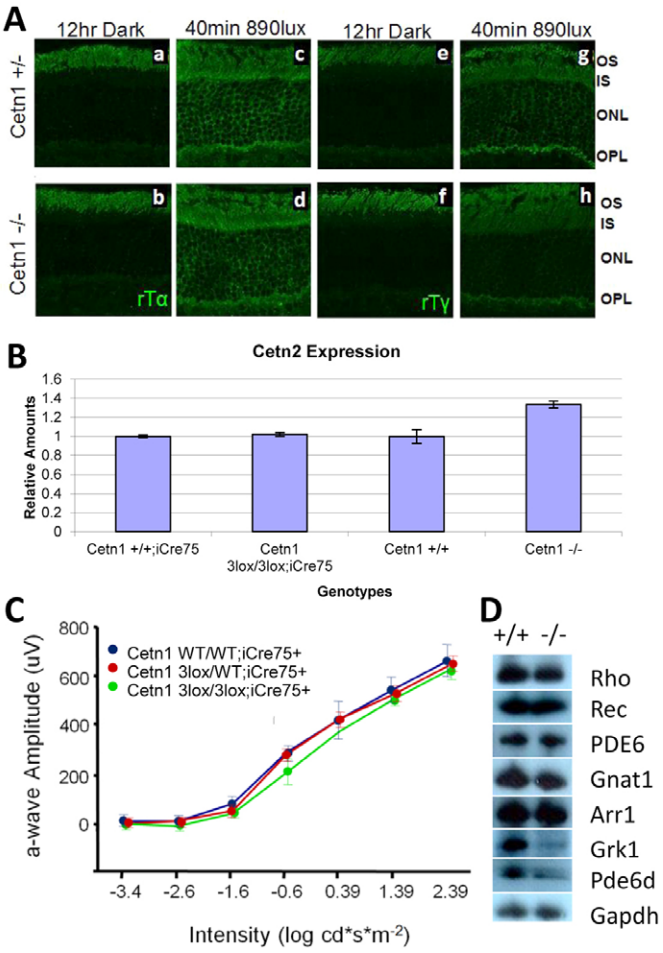

Fig. 2. Normal transducin translocation and phototransduction in *Cetn1*$^{-/-}$ photoreceptors. (**A**) Light-induced translocation of transducin subunits, Tα and Tβγ. *Cetn1*$^{+/-}$ and *Cetn1*$^{-/-}$ mice were dark-adapted for 12 hours, or dark-adapted and exposed to light for 40 minutes. Retina cryosections were probed with anti-transducin antibodies, anti-Gnat1(Tα) and anti-Gngt1 (Tγ). Light-induced translocation of Tα and Tγ was indistinguishable in the two genotypes. (**B**) Upregulation of CETN2 in *Cetn1*$^{-/-}$ knockout retinas. cDNA from *Cetn1*$^{WT/WT}$;*iCre75+*, *Cetn1*$^{3lox/3lox}$;*iCre75+*, *Cetn1*$^{+/+}$, and *Cetn1*$^{-/-}$ retinas was amplified under real-time conditions (see Materials and Methods). No significant difference in *Cetn2* expression was detected in *Cetn1*$^{3lox/3lox}$;*iCre75+* ($N=2$) compared with WT retinas. In global knockouts, *Cetn2* was upregulated over 30% ($N=2$) suggesting compensation for loss of the CETN1 isoform. (**C**) Electroretinogram of wild-type, heterozygous and homozygous *Cetn1* rod-specific deletion retinas. (**D**) Immunoblots of outer segment polypeptides unaffected (rhodopsin, recoverin, PDE6, rod Tα, and rod arrestin), and downregulated (GRK1 and PDE6D) by *Cetn1* deletion.

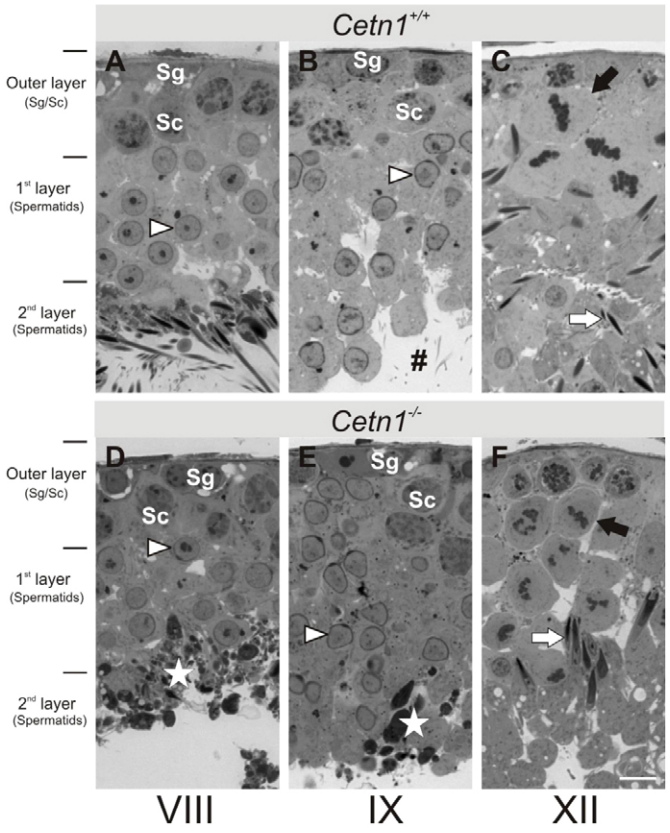

Fig. 3. Seminifereous tubules of *Cetn1*$^{+/+}$ and *Cetn1*$^{-/-}$ mice. Stage-matched seminifereous tubules from (**A–C**) *Cetn1*$^{+/+}$ mice and (**D–F**) *Cetn1*$^{-/-}$ mice. The outer layer consists of spermatogonia (Sg) and spermatocytes (Sc), the first layer consists of spermatids (arrowheads) from round Golgi phase to the end of acrosome phase; the second layer harbors the maturating spermatids up to spermiation into the lumen of seminifereous tubules. (A) Stage VIII tubules of *Cetn1*$^{+/+}$ mice with spermatocytes in the outer layer, round spermatids in the first layer and tailed spermatids in the second layer at the luminal side of the tubules. (B) Stage IX tubules of *Cetn1*$^{+/+}$ mice. Instead of round spermatids, capped spermatids entering acrosome phase are present in the first tubule layer. #, Tails of mature spermatids after spermiation in the tubule lumen. (C) Stage XII tubules of *Cetn1*$^{+/+}$ mice exhibit spermatocytes at meiosis (black arrow) in the first layer forming the new generation of spermatids. Elongated spermatids (white arrow) are present in the second layer. (D) Stage VIII tubules of *Cetn1*$^{-/-}$ mice with spermatocytes in the outer layer, and round spermatids in the first layer. Tailed spermatids in the second layer are absent, but dark, dense material of degraded spermatids (white star) is present. (E) Stage IX tubules of *Cetn1*$^{-/-}$ mice reveal the same layering as *Cetn1*$^{+/+}$ mice, but contain dark dense material of degraded spermatids (white star). (F) Stage XII tubules of *Cetn1*$^{-/-}$ mice show spermatocytes during meiosis (black arrow) in the first layer and elongated spermatids at the transition to maturation phase (white arrow). Layering of the seminifereous tubules was the same in *Cetn1*$^{+/+}$ and *Cetn1*$^{-/-}$ mice. Scale bar: 10 µm.

Cetn1$^{-/-}$ sperm number is reduced

Mature sperm in semen extracted from equal amounts of spermatic ducts of *Cetn1*$^{+/+}$, *Cetn1*$^{+/-}$ and *Cetn1*$^{-/-}$ mice were quantified (Fig. 4). While no difference in number, shape, length and motility of *Cetn1*$^{+/+}$ and *Cetn1*$^{+/-}$ sperm (Fig. 4A,B) could be ascertained, *Cetn1*$^{-/-}$ sperm were reduced in number by 99% (supplementary material Table S1) and malformed. *Cetn1*$^{-/-}$ sperm malformation was heterogeneous, i.e. heads

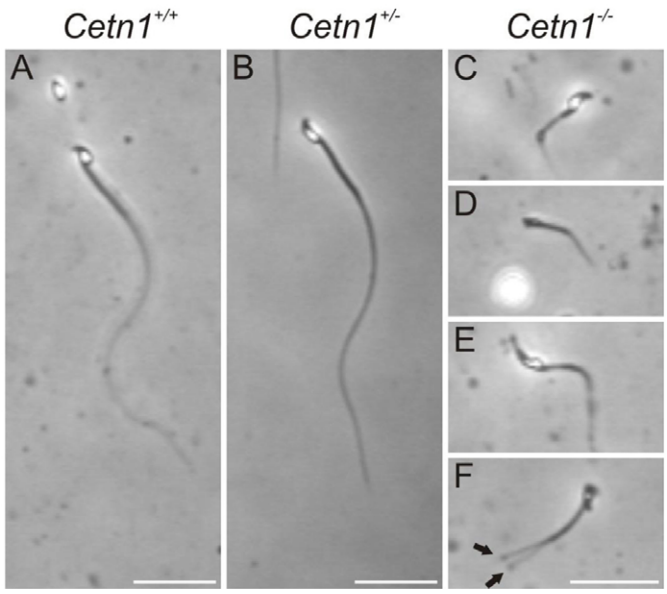

Fig. 4. Light microscopy analysis of sperm present in spermatic duct. Equal amounts of sperm from *Cetn1*$^{+/+}$, *Cetn1*$^{+/-}$ and *Cetn1*$^{-/-}$ mice were collected and analyzed by light microscopy. (**A**,**F**) Sperm extracted from *Cetn1*$^{+/+}$ and *Cetn1*$^{+/-}$ mice were identical in shape and length. (**B–E**) Sperm from *Cetn1*$^{-/-}$ mice were all malformed in one or more ways: sperm tail shape, sperm tail length, head shape and midpiece. Bifurcated tail-like structures (F, arrows) were sometimes observed. Scale bars: 25 µm.

were incorrectly formed, midpieces were shortened, and tails were shortened and occasionally forked. Of the few sperm found in *Cetn1*$^{-/-}$ semen, all were immotile, malformed (Fig. 4C–F) and, without exception, revealed hallmarks of oligoteratozoospermia.

Cetn1$^{-/-}$ spermiogenesis is impaired in late steps of elongated spermatid maturation

Next, we examined *Cetn1*$^{-/-}$ and *Cetn1*$^{+/+}$ testes by transmission electron microscopy in depth. No structural anomaly of diploid spermatocytes, round spermatids post-meiosis (supplementary material Fig. S3A,B; Fig. S4A,B), or sperm heads was observed during early elongation (supplementary material Fig. S3C,D). In addition, we did not detect any structural alterations in the centriole arrangement or the basal body apparatus in post-meiotic round spermatids of the early spermiogenesis (supplementary material Fig. S4A–D). For example, there was no difference in the diameter of the centrioles in *Cetn1*$^{-/-}$ (average of 205 nm; $n=5$) compared to *Cetn1*$^{+/+}$ spermatids (average of 207 nm; $n=5$).

First differences between *Cetn1*$^{-/-}$ and *Cetn1*$^{+/+}$ spermatids became apparent during the early maturation phase of spermiogenesis, steps 13–14 (Fig. 5). Typically, elongating spermatids are engulfed by the acrosome to the nuclear caudal pole and straight, parallel membrane systems form with contributions from nuclear, acrosomal and Sertoli cell ectoplasmic specialization membranes, the latter of which is associated with the spermatid via specialized cell-cell contacts (Fig. 5A). In *Cetn1*$^{-/-}$ mice the caudal movement of the acrosome was heterogeneously altered, and interspaces between the Sertoli cell ectoplasmic specialization and plasma membranes became frequent (Fig. 5B, black bar). Thus, *Cetn1*$^{-/-}$ spermatid acrosomes appeared malformed compared to controls. This

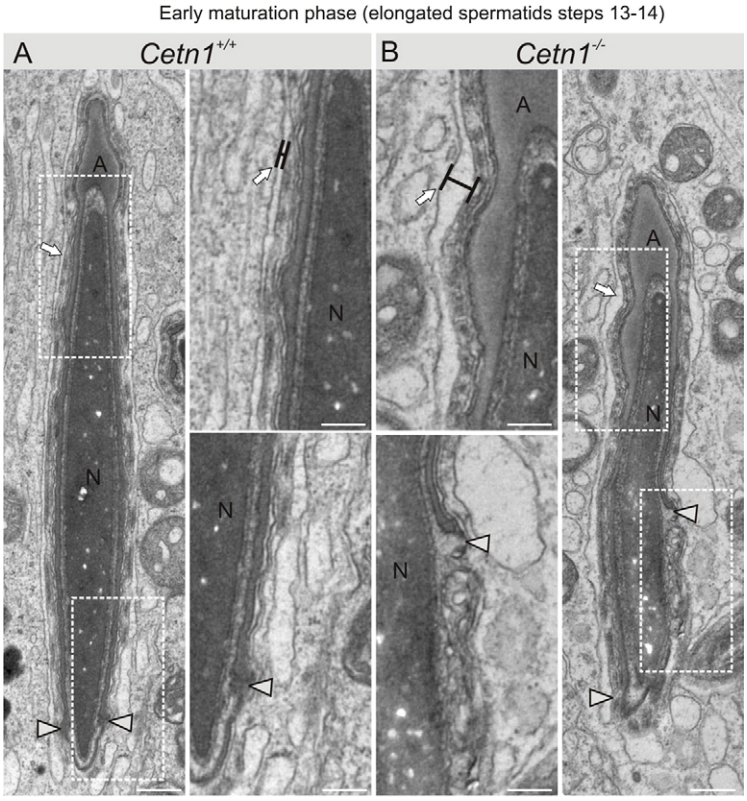

Fig. 5. Ultrastructure of early maturation phase spermiogenesis of *Cetn1*$^{+/+}$ and *Cetn1*$^{-/-}$ spermatids. (**A**,**B**) The first differences between *Cetn1*$^{+/+}$ and *Cetn1*$^{-/-}$ were found in steps 13–14. The caudal movement of the acrosome forming the acrosomic clefts (arrowheads) was uneven and a general bulky appearance was observed in *Cetn1*$^{-/-}$ spermatids. Sertoli cell membranes were deformed compared to the straight, parallel membranes of *Cetn1*$^{+/+}$ mice (arrows). At higher magnification (center two panels), wider distention between the Sertoli cell membranes was seen (arrows, black bars). Also at high magnification, at the spermatid base a disruption to the caudal migration of the acrosome was evident (B, arrowheads). Scale bars: 0.5 μm.

membrane malformation worsened gradually during spermiogenesis steps (supplementary material Fig. S5) until in late maturation phase (steps 15–16), abnormalities associated with spermiogenesis in *Cetn1*$^{-/-}$ male mice were drastic and prominent (Fig. 6). In most *Cetn1*$^{-/-}$ spermatids, tails were absent or, if present, misshapen (Fig. 6B,C; supplementary material Fig. S4F); nuclei of *Cetn1*$^{-/-}$ spermatids were often bifurcated with chromatin appearing dysmorphic (Fig. 6B,C). The few spermatids that remained were embedded in electron-dense perforated granules, indicating cell degradation.

Spermiogenesis involves rearrangement of the spermatid centrosome, forming the basal body apparatus, which facilitates the functional connection between spermatid nucleus and sperm flagellum. Rearrangements start in the early round spermatid with its first axonemal projection, persist throughout acrosome phase until the proximal centriole of the striated body is enclosed by the nuclear fossa, and are completed by release of sperm after centriole reduction. Since spermatid centriolar/centrosomal rearrangements are well established, we examined the spatial distribution of centrioles during spermiogenesis. To achieve this, we double-labeled cryosections of wild-type and mutant seminifereous tubules with CETN1-specific antibodies and with antibodies directed against CETN3 to serve as a centriolar marker (supplementary material Figs S6, S7; Fig. 7). We detected CETN1 and CETN3 in all germ cell types and all seminifereous tubule layers of adult *Cetn1*$^{+/+}$ testis in the form of double or single dots representing centrioles of centrosomes, corresponding to different cell cycle phases of the germ cells (supplementary material Fig. S6A, Fig. S7A–D). As expected in *Cetn1*$^{-/-}$ testes, CETN1 labeling was absent while CETN3 labeling was present

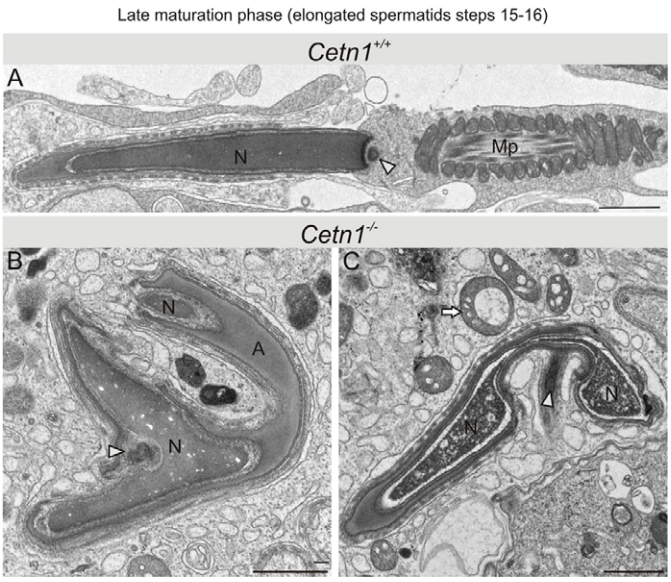

Fig. 6. Late maturation phase spermatids. Spermatids were analyzed by high resolution electron microscopy at steps 15–16 of spermiogenesis. (**A**) Wild-type spermatid showing a midpiece (Mp), an elongated nucleus (N) and a remaining centriolar structure (arrowhead). (**B**,**C**) Abnormalities were prominent in *Cetn1*$^{-/-}$ spermatids. No midpiece or tail formation was found. Nuclei were split, bifurcated and the chromatin appeared perforated. Additionally, spermatid heads were bent over and the shape of the centrosomal region (arrowheads) was abnormal. Cell debris of spermatids in granules (C, arrow) was observed, indicating cell degeneration. A, acrosome. Scale bars: 1 μm.

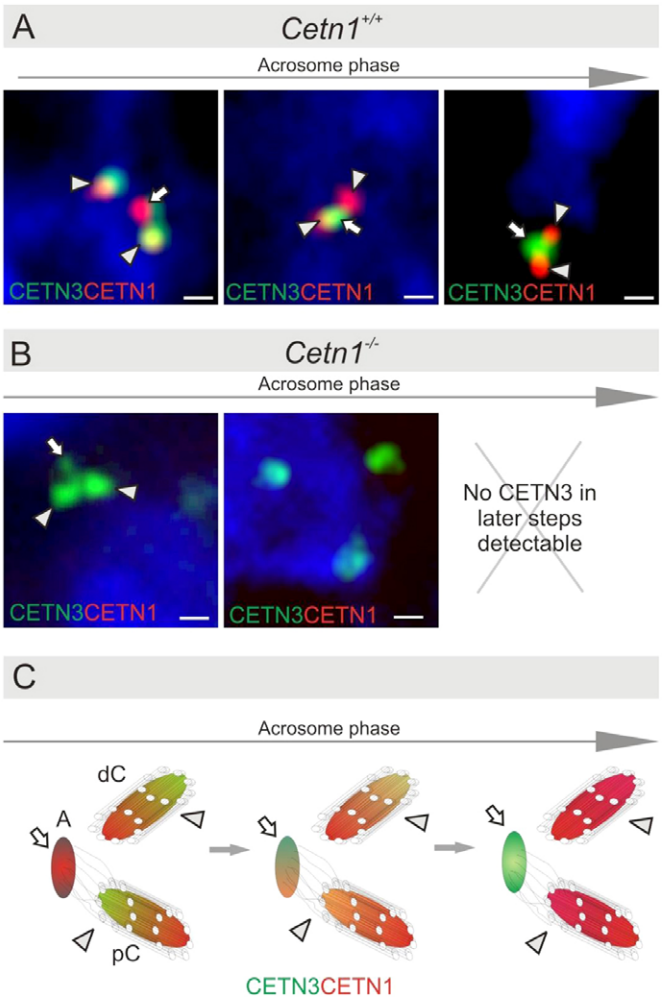

Fig. 7. CETN1 expression during centriole rearrangement in spermatids in late spermiogenesis. (**A**,**B**) Centrin expression was detected by immunofluorescence. Double-labeling of CETN1 (red) and the centriole marker CETN3 (green) in acrosome phase spermatids (steps 8–12) of *Cetn1*$^{+/+}$ and *Cetn1*$^{-/-}$ mice. (A) CETN1 and CETN3 were colocalized in the centrioles of spermatid centrosomes, the distal and the proximal centrioles (arrows) of the sperm flagellar basal apparatus as well as the centriolar adjunct (arrowheads) in *Cetn1*$^{+/+}$ mice. (B) CETN1 was absent, centriole arrangement of the flagellar basal apparatus was disorganized and spermatogenesis was arrested in the last phase in *Cetn1*$^{-/-}$ mice. No CETN3 staining was identified in later steps of spermiogenesis (indicated by the X). (**C**) Scheme representing the polarization of CETN3/CETN1 during the acrosome phase; A, adjunct; dC, distal centriole; pC, proximal centriole; arrows and arrowheads as in A. Scale bars: 0.5 µm.

(supplementary material Fig. S6B; S7E–H). Interestingly, in *Cetn1*$^{+/+}$ acrosome phase spermatids, we observed centriole labeling patterns as CETN1- and CETN3-positive fluorescent dots arranged in triads (Fig. 7) which correspond to the centriole pair and the centriolar adjunct, previously described as an extension of the proximal centriole with centriolar characteristics (Fouquet et al., 1998; Manandhar et al., 1998; Zamboni and Stefanini, 1971).

During maturation of *Cetn1*$^{+/+}$ spermatids CETN1 label faded from the centriole adjunct while CETN3 labeling decayed in the two centrioles, but persisted in the centriole adjunct (Fig. 7A). The triad arrangement of the two centrioles and centriolar adjunct was initiated during the early acrosome phase of *Cetn1*$^{-/-}$ spermatids (Fig. 7B, left panel). However, during acrosome progression and spermatid elongation, labeling of the centriolar marker disappeared not only in the centrioles but also in the adjunct (Fig. 7B, middle and right panels), indicating the degradation of the two centrioles and the centriolar adjunct during *Cetn1*$^{-/-}$ sperm head elongation. No further difference in labeling pattern using anti-CETN3 antibodies was observed in either spermatogonia (supplementary material Fig. S7A,E) or spermatocytes (supplementary material Fig. S7B,F).

Cetn1$^{-/-}$ basal body complex degrades prior to flagellar outgrowth

Next we analyzed spermatids during late spermiogenesis in 150 nm-thick sections through testes of *Cetn1*$^{-/-}$ and *Cetn1*$^{+/+}$ mice by transmission electron microscopy (Fig. 8). The proximal centriole differentiates into the striated body anchored within the nuclear fossa, while the distal centriole forms the basal body from which the flagellar axoneme extends (Fig. 8B). We identified the centriole pair and centriolar adjunct of the basal body apparatus (Fig. 8A,C) of *Cetn1*$^{-/-}$ and *Cetn1*$^{+/+}$ spermatids by correlating the dots stained by anti-centrin antibodies in our previous immunofluorescence experiments (Fig. 7). Absent CETN1, centrioles of the differentiating basal body apparatus failed to contact the nuclear membrane/envelope (Fig. 8C) and a gap between the nucleus and basal body apparatus persisted during further maturation (Fig. 8C,D). Consequently the nuclear fossa was deformed in most *Cetn1*$^{-/-}$ spermatids (Fig. 8C,D). As striated and basal bodies were not formed, the entire basal body complex was reduced and apparently degraded prior to flagellar outgrowth (Fig. 8D). Dimensions of the centrioles and basal bodies of mature spermatids revealed no difference in the centriole diameter between *Cetn1*$^{+/+}$ and *Cetn1*$^{-/-}$ [average diameters of 205 nm (n=5) and 202 nm (n=3), respectively]. The basal body length [average 491 nm (n=4)] in mature *Cetn1*$^{+/+}$ spermatids was comparable to normal centrioles. However, the basal body length was variable and reduced to 250–160 nm (n=3) in the last steps of *Cetn1*$^{-/-}$ spermatid maturation. Nonetheless, we observed *Cetn1*$^{-/-}$ spermatids bearing a flagellum infrequently (1:500). In these cases, the structure of basal body complex (including a rudimentary striated body) was disturbed and a gap between the remnants of the basal body complex and nucleus was present (supplementary material Fig. S4F).

Discussion

Yeast (*Saccharomyces cerevisiae*) and algae (e.g. *Chlamydomonas reinhardtii*) each express a single centrin termed Cdc31 and VFL2 (variable flagellar number 2), respectively. Other single cell protozoa such as the ciliates *Paramecium* and *Tetrahymena* express multiple centrin isoforms (Zhang and He, 2012). By sequence comparison, CETN1 and CETN2 are closely related to VFL2, while CETN3 is closer to Cdc31 (Middendorp et al., 1997). VFL2 is localized to the stellate structure of the flagellar transition region, nucleus-to-basal body connectors and fibers connecting basal bodies. Centrin-deficient *vfl2* mutants exhibit defects in basal body replication, maturation and flagella numbers (Koblenz et al., 2003; Salisbury et al., 1988; Taillon et al., 1992). In *Chlamydomonas*, increase in intracellular Ca^{2+} leads to a contraction of centrin-containing fibers of the

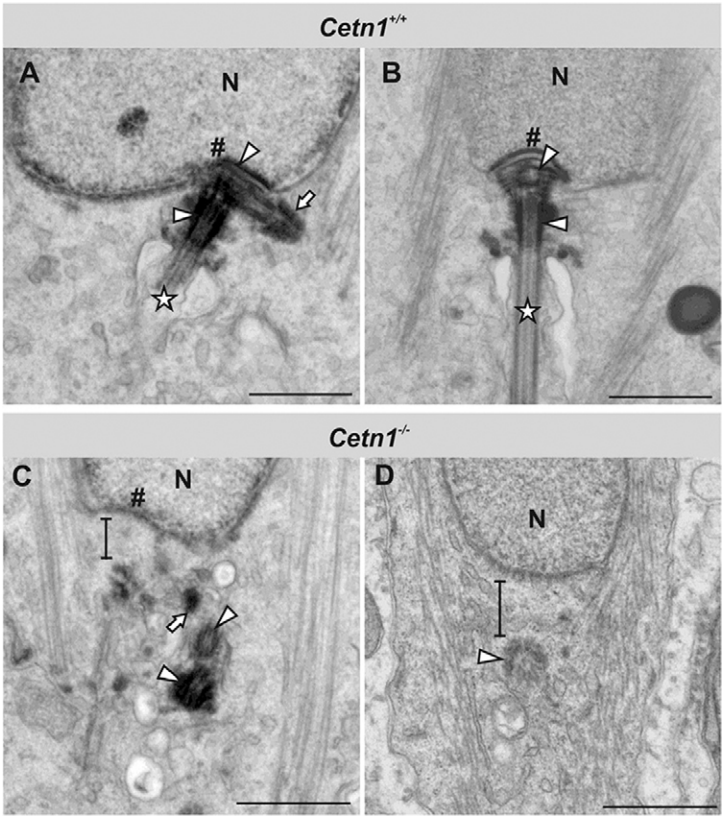

Fig. 8. Ultrastructure of spermatid centriole rearrangement during late spermiogenesis. (**A**,**B**) *Cetn1*$^{+/+}$ spermatids during centriole rearrangement of late spermiogenesis. (A) Proximal and distal centrioles (arrowheads) positioned directly adjacent to the fossa (#) of the nucleus (N). The proximal centriole projects the adjunct (arrow), and the sperm flagellum axoneme is visible (star). (B) Rearranged centrioles (arrowheads) finish to form the basal body apparatus at the nuclear fossa (#), from which the sperm flagellar axoneme extends (star). (**C**,**D**) *Cetn1*$^{-/-}$ spermatids during centriole rearrangement. (C) Both centrioles (arrowheads) and the adjunct remnant (arrow) appear disengaged from the nuclear membrane, as indicated by the black bar. The nuclear fossa (#) is dysmorphic. (D) The distal centriole (arrowhead) projects a tubular structure corresponding to the axoneme, but it is bent and flaccid. Instead of a modified proximal centriole, a cytoplasmic gap (indicated by black bar) appears between the nucleus (N) and the distal centriole. Scale bars: 0.5 μm.

flagellar rootlet, a process that leads to excision of the flagellum (Sanders and Salisbury, 1989).

Mouse CETN1 is a Ca^{2+}-binding protein with four EF-hand motifs (EF1–4). Only EF3–4 are considered functional, high-affinity Ca^{2+}-binding sites (Trojan et al., 2008). In mouse, CETN1 expression is restricted to ciliated cells, including male germ cells and photoreceptors where it located in the connecting cilium (Fig. 1G) along the inner surface of the microtubule doublets (Trojan et al., 2008). By contrast, CETN2 and CETN3 are expressed in all retina neurons, and are present at both connecting cilia and centrioles of photoreceptors (Trojan et al., 2008). Screening with a Ca^{2+}-activated CETN1 identified the photoreceptor transducin Tβγ-subunit (Gnb1/Gng1) as an interacting partner. This interaction was confirmed by GST pulldown, co-sedimentation, size exclusion chromatography and light-scattering experiments. CETN1 was therefore hypothesized to regulate light-dependent translocation of membrane-associated transducin (Giessl et al., 2006; Trojan et al., 2008). However, as shown (Fig. 2), deletion of murine CETN1 had no consequence on transducin localization suggesting that other centrin isoforms may substitute for CETN1 loss.

We observed upregulation of CETN2 on the RNA level in the absence of CETN1 (Fig. 2B). Based on sequence similarity and CETN1/CETN2 colocalization in the connecting cilium, CETN2 may substitute for CETN1 and prevent a transducin mislocalization phenotype. We observed further that CETN1 deletion reduced the levels of PDE6δ and GRK1 in photoreceptors (Fig. 2D). PDE6δ forms a soluble complex with prenylated GRK1 and regulates transport of GRK1 to rod and cone outer segments (Zhang et al., 2007). Downregulation of the complex in *Cetn1*$^{-/-}$ suggests that CETN1 may participate in the trafficking of GRK1 through the cilium directly, or mediate the assembly of GRK1-containing cargo which then moves by intraflagellar transport.

The most prominent *Cetn1*$^{-/-}$ phenotype was male infertility. CETN1 is highly expressed in testes (Hart et al., 1999; Wolfrum and Salisbury, 1998) and our present analysis of *Cetn1*$^{-/-}$ male infertility provides evidence that CETN1 is required for spermatid maturation. We observed CETN1 expression in all germ cell types of *Cetn1*$^{+/+}$ seminifereous tubule layers, in addition to the outer layer (Tanaka et al., 2010). *Cetn1*$^{-/-}$ spermatids appeared to differentiate correctly until the late acrosome to early maturation phase, indicating that CETN1 may not be required for meiosis as previously hypothesized (Hart et al., 1999). First differences between *Cetn1*$^{-/-}$ and *Cetn1*$^{+/+}$ mice were detected during the early maturation phase of haploid spermatids (spermiogenesis steps 13–14; Fig. 5), as evidenced by arrested movement of the acrosome angle and disturbed adhesion complexes at the ectoplasmic specialization of Cetn1$^{-/-}$ spermatids. CETN1 either may participate directly in these processes or may determine the complex cytoskeletal arrangement necessary for spermatid differentiation. However. more prominent abnormalities became obvious in the late *Cetn1*$^{-/-}$ maturation phase, e.g. bent spermatid heads (Fig. 6B,C). Additionally, *Cetn1*$^{-/-}$ spermatids failed to develop correct tails or midpieces, and flagella were severely deformed or absent.

Our fluorescence and ultrastructural analyses of *Cetn1*$^{-/-}$ spermatids reveal that CETN1 is essential for centriole rearrangement and correct formation of the basal body apparatus in haploid male germ cells (Fig. 7). Interestingly, localizations of CETN1 and CETN3 in centriolar structures

changed dynamically during these processes. Comparable molecular dynamics of maturing spermatids were demonstrated previously for γ-tubulin by immunofluorescence and immunoelectron microscopy (Manandhar et al., 1998). Present data indicate that CETN1 functions to establish the basal-body–nucleus attachment within the nuclear fossa (Fig. 8), consistent with previous studies of the basal body apparatus and the basal-body–nucleus connectors described in unicellular green algae (Brugerolle and Mignot, 2003; Harper et al., 1993; Wright et al., 1985). As centrins are major components of the basal-body–nucleus connectors in green algae, absence of centrin in the *Chlamydomonas* vfl-2 mutant alters flagellogenesis (Harper et al., 1993; Wright et al., 1985). A role of the basal-body–nucleus connector in the assembly of polarized microtubule arrangements has been discussed for green algae (Brugerolle and Mignot, 2003). The disturbed microtubule system may be a plausible explanation for defects observed in the early spermiogenesis maturation phase of *Cetn1*$^{-/-}$ spermatids (e.g. correct caudal movement of the acrosome; Fig. 5), for the malformed spermatids in the maturation phase (Fig. 6) and ultimately, for the few and immotile sperm found in *Cetn1*$^{-/-}$ semen (Fig. 4). Our data provide first evidence for centrin participation in formation of basal-body–nucleus connectors and flagellogenesis in mammals, a function which is conserved evolutionarily from unicellular green algae to vertebrates.

Male infertility is a common consequence of ciliopathies that display syndromic characteristics (Escalier, 2006). Prominent among these are deletions of genes related to the multi-syndromic Bardet–Biedl syndrome (BBS) or nephronophthisis (NPHP) genes. In male *Bbs1*$^{-/-}$, *Bbs2*$^{-/-}$, *Bbs4*$^{-/-}$ and *Bbs6*$^{-/-}$ mice, spermatozoa heads were present but flagella were completely absent (Davis et al., 2007; Fath et al., 2005; Mykytyn et al., 2004; Nishimura et al., 2004). Molecular analysis revealed that the BBS proteins form a functional complex, the BBSome, which is essential for ciliogenesis or flagella outgrowth (Nachury et al., 2007). BBS knockouts manifest a broad syndromic phenotype which includes retinal degeneration, obesity, development of renal cysts, and olfactory abnormalities, among others. Deletion of the nephrocystin-4 gene (*Nphp4*) leads to infertility caused by sperm immobility paired with retina degeneration (Won et al., 2011), while deletion of nephrocystin-1 is associated with defects in spermiogenesis at much earlier steps (Jiang et al., 2008). Here we show that *Cetn1*$^{-/-}$ spermatid development is affected after the cap phase, namely at the transition from late acrosome phase to the early maturation phase of spermiogenesis, producing an altered rearrangement of the two centrioles and the centriolar adjunct, the effects of which manifest later as dysmorphic spermatid heads and tails. This is a unique finding among mouse models of male infertility. Additionally, the *Cetn1*$^{-/-}$ mouse phenotype is nonsyndromic and testis-specific, indicating that CETN1 performs an essential role in spermiogenesis that cannot be compensated by centrin isoform redundancy.

A screen of centrins from published sequences reveals that CETN2 retroposed as CETN1 is unique to mammals, indicating a highly conserved role of centrins in centrosome or centriole function. The *Cetn2* gene is one of fourteen genes expressed in every centriole-containing cell (Hodges et al., 2010) with the only known exception being haploid male germ cells (Tanaka et al., 2010), which are the only known cells affected by *Cetn1* deletion. Our data suggest that CETN1 absence may be compensated by the CETN2 isoform in diploid ciliated cells, while in haploid germ cells this molecular redundancy of centrin isoforms is absent when the X-chromosomal linked CETN2 is silenced by meiotic sex chromosome inactivation (MSCI) (Hart et al., 2001; Turner, 2007). Retrotransposition from X-linked genes was proposed to be enhanced by highly selective pressure caused by MSCI in spermatogenesis (McCarrey et al., 1992) and an equivalent scenario was described for the sperm-specific phosphoglycerate kinase PGK2 and the ubiquitous X-linked PGK1 (Danshina et al., 2010; McCarrey et al., 1992), which are not involved in sperm tail formation. As in lower organisms, mammalian CETN1 and CETN2 likely participate in basal body function and flagellar formation with presence of one isoform being required for proper centriole and/or centrosome function.

Materials and Methods

Mice

WT (C57BL/6J) mice and EIIa-cre mice were purchased from The Jackson Laboratory (Bar Harbor, ME). All animal experiments were approved by the Institutional Animal Care and Use Committees (IACUC) at the Universities of Utah and Mainz.

Generation of *Cetn1* floxed mice

A three *loxP* strategy was used in the *Cetn1* knock-in construct. A chromosome 18 BAC clone (RP24-177G6, 154,555 bp insert) containing the *Cetn1* gene was acquired from the Children's Hospital Oakland Research Institute (CHORI, Oakland, CA). The *Cetn1* gene contains a coding exon and an untranslated 3′-UTR exon. Primers outside *Kpn*I and *Eco*RI sites surrounding the *Cetn1* gene were used to amplify the 12 kb genomic region. A 5466 bp *Kpn*I–*Cla*I fragment was cloned into the pBS-SK+ vector (Stratagene). A *loxp+Xho*I linker with *ApaI* overhangs on both ends was generated by annealing two oligonucleotides: ApaLoxXhoApa.F, 5′-cataacttcgtataatgtatgctatacgaagttatctcgaggggcc-3′, and ApaLoxXhoApa.R, 5′-cctcgagataacttcgtatagcatacattatacgaagttatgggcc-3′. The double-stranded construct was cloned into the unique *Apa*I site upstream of exon 1. The 3,884 bp *Cla*I–*Cla*I fragment downstream of exon1 was cloned into the construct next to complete the homologous region. Finally, a floxed neo cassette was inserted into the unique *Spe*I site. The neo cassette contained a DNA polymerase II promoter driving the neomycin resistance gene. The final construct containing a floxed exon 1 and floxed neo cassette (total 3*loxps*), completely sequenced for verification, was linearized with *Kpn*I prior to electroporation. 480 ES cell clones were screened by PCR for correct targeting of the short arm of recombination as well as the 5′ *loxP* in the long arm of recombination. Twenty of the 480 clones showed correct recombination. Of the 20 positives, two of the correct ES cells were microinjected into blastocysts for production of chimeric offspring.

Genotyping

Cetn1$^{3lox/WT}$;*iCre75*$^{+}$, *Cetn1*$^{3lox/3lox}$; *iCre75*$^{+}$, *Cetn1*$^{+/-}$, and *Cetn1*$^{-/-}$ mice were genotyped with the following primers. 5′loxPF: 5′-tgctttggttcccagaagg, P1F: 5′-cacacagaacctggactttagc-3′, and P3R: 5′-cctgggtatggtagtgatgaac-3′. P1F/P3R amplify a 418 bp WT fragment, and 5′loxPF/P3R a 173 bp knockout fragment. *Cetn1* RT-PCR in testes was performed using the following primers. MmCen1 RT holo F: 5′-atggcgtccaccttcaggaag-3′ and MmCen1 RT holo R: 5′-ttaataaaggttggtctttttc-3′. Intron-spanning GAPDH primers were used as controls. GAPDH forward: 5′-cctcgtcccgtagacaaaatg-3′ and GAPDH reverse: 5′-tgaaggggtcgttgatggc-3′.

Antibodies

Anti-rhodopsin, anti-cone arrestin, anti-rod arrestin, anti-cone PDE6α′; anti-R9AP; anti-GC1, anti-GRK1; anti-rod Tα, anti-rod Tγ; anti-M/L-opsin; anti-peripherin/RDS; anti-coneTα, anti-CNGA1, anti-CNGA3; anti-cone Tγ, anti-PDE6, and anti-centrin antibodies (MmC1, CSUW 11-7) have been described previously (Baehr et al., 2007; Giessl et al., 2004; Zhang et al., 2008). Polyclonal rabbit MmC1 was preadsorbed with bacterially expressed mouse CETN2/3/4 proteins until no MmC1 CETN2/3/4 complexes were detectable in the immunoprecipitate.

Confocal microscopy of retina sections

Eyes from mice of various ages were harvested under dim red light following overnight dark-adaptation, or after exposure to light (890 lux) for 40 minutes. Eyes were fixed and processed as described (Avasthi et al., 2009). Cryosections were blocked in 10% normal donkey serum in 0.1 M phosphate buffer including 0.1% Triton X-100 (PBT) for 1 hour, and incubated with primary antibody diluted in PBT overnight in a rotating humidified chamber at 4℃. After washing the sections, FITC-conjugated secondary antibody was co-applied with propidium iodide (Invitrogen Molecular Probes^{TM}). The sections were imaged using an Olympus

Fluoview (FV 1000) inverted confocal microscope (supplementary material Fig. S1).

Real-time PCR

Quantitative PCR was performed using total RNA from one month-old wild-type (WT), *Cetn1*$^{3lox/3lox}$;*iCre75+*, or *Cetn1*$^{-/-}$ retinas. The following primers were used: *Cetn1*mRNA.F2: 5′-aagcaagaagttcgggaagcc-3′, *Cetn1*mRNA.R2: 5′-gagtcatcacagccaagaagtcattg-3′, Cetn2mRNA.F: 5′-agggcagaacaagagcacatag-3′, Cetn2mRNA.R: 5′-atggatacatggacaactaagaagcc-3′, GAPDHqPCR2.F: 5′-taccccaatgtgtccgtcgtg-3′, GAPDHqPCR3.R: 5′-ttgagagcaatgccagcccc-3′. *Cetn1* primers are located in exon1 and *Cetn2* primers are located in the 3′UTR in exon 4. RNA was reverse transcribed using random hexamers by the Superscript III First Strand Synthesis Kit (Invitrogen Corp., Carlsbad, CA). A validation experiment was run using fivefold dilutions of WT cDNA standards. Once amplification efficiencies were confirmed to be approximately equal (slope of log input amount versus $\Delta C_T < 0.1$), WT and mutant retinas were compared for levels of *Cetn1* and *Cetn2* gene expression using the comparative C_T method for relative quantitation.

Preparation of sperm

Semen of mouse testes was harvested by squeezing spermatic ducts into 500 µl BTS buffer (0.1 M sodium bicarbonate, 0.05% Tween 20, 300 mM NaCl, pH 8). Sperm were counted in a standard count chamber (20 µm, Leja Products B.V., Niew Vennep, The Netherlands).

Testis preparation and immunofluorescence microscopic analysis

Testes were cryofixed in melting isopentane and cryosectioned as described (Wolfrum and Salisbury, 1998). Primary antibodies were visualized by Alexa-Fluor-488- or Alexa-Fluor-568-conjugated secondary antibodies (Invitrogen Molecular Probes™), and DAPI was used to stain nuclear DNA. Leica DM 6000 B microscope images (Leica Microsystems, Bensheim, Germany), were processed with Adobe Photoshop CS (Adobe Systems Inc., San Jose, CA, USA).

Conventional fixation and transmission electron microscopy

Dissected testes were fixed in cacodylate-buffered glutaraldehyde and osmium tetroxide followed by Renlam® M-1 resin (Serva, Heidelberg, Germany) as described (Sedmak and Wolfrum, 2011). Semi thin sections (1 µm thick) were cut, contrasted with methylene blue and azure B, and viewed with a Leica DM 6000B microscope (Leica Microsystems, Bensheim, Germany). Ultrathin sections were analyzed in a Tecnai 12 BioTwin transmission electron microscope (FEI, Eindhoven, NL) and imaged using a CCD camera (SIS MegaView3, Surface Imaging Systems, Herzogenrath, Germany) and Analysis Imaging Interface (FEI, Eindhoven, NL). Images were processed with Adobe Photoshop CS. For quantification, germ cells were counted in 100×50 µm rectangles of stage IX seminifereous tubule semithin sections. Reproductive epithelia thickness was measured with Leica Applications Suite (Leica Microsystems, Bensheim, Germany).

Western blotting

Testes total protein lysate (40 µg) was separated by SDS-PAGE (15% acrylamide) and transferred to PVDF membrane (Millipore Corporation, Billerica MA, USA) using a semidry blotter (BioRad, München, Germany). Membranes were blocked in milk, washed and incubated overnight with pre-adsorbed MmC1 primary antibody (1:50 dilution) at room temperature with shaking. After washing, the membranes were incubated in secondary anti-rabbit antibody (1:15000 dilution; VWR International, Darmstadt, Germany). The membranes were washed further and incubated with ECL reagent (GE Healthcare, Solingen, Germany). Luminescence was visualized by photographic film (Kodak GMBH, Stuttgart, Germany).

Acknowledgments

The authors thank Dr Günther Kamp for his advice on semen preparations, and Elisabeth Sehn for her skillful technical support in electron microscopy.

Author contributions

P.A. generated and G.Y. maintained the Cetn1$^{-/-}$ mice; P.A. performed retina immunohistochemistry; J.F.S. performed immunofluorescence of testes, semen analysis and transmission electron microscopy; P.A., W.B., U.W. designed experiments; J.M.F., W.B. and U.W. wrote the paper.

Funding

This work was supported by the National Institutes of Health [grant numbers EY08123, EY019298 to W.B.]; a core grant from the National Eye Institute [grant number EY014800-039003] to the Moran Eye Center; the Deutsche Forschungsgemeinschaft [grant number Wo 548/6 to U.W.]; ProRetina Deutschland e.V. [grant number 5/2011 to U.W.]; the FAUN-Stiftung, Nűrnberg [grant number 6/2007 to U.W.]; the European Community [grant number FP7/2009/241955 (SYSCILIA) to U.W.]; Landesgraduiertenförderung Rheinland Pfalz [grant number 5/2009 to J.F.S.]; and a Johannes Gutenberg-Universitaet Forschungsförderung S1 [grant number S1 3-2009 to U.W.]. Deposited in PMC for release after 12 months.

Supplementary material available online at
http://jcs.biologists.org/lookup/suppl/doi:10.1242/jcs.128587/-/DC1

References

Avasthi, P., Watt, C. B., Williams, D. S., Le, Y. Z., Li, S., Chen, C. K., Marc, R. E., Frederick, J. M. and Baehr, W. (2009). Trafficking of membrane proteins to cone but not rod outer segments is dependent on heterotrimeric kinesin-II. *J. Neurosci.* **29**, 14287-14298.

Baehr, W., Karan, S., Maeda, T., Luo, D. G., Li, S., Bronson, J. D., Watt, C. B., Yau, K. W., Frederick, J. M. and Palczewski, K. (2007). The function of guanylate cyclase 1 and guanylate cyclase 2 in rod and cone photoreceptors. *J. Biol. Chem.* **282**, 8837-8847.

Brugerolle, G. and Mignot, J. P. (2003). The rhizoplast of chrysomonads, a basal body-nucleus connector that polarises the dividing spindle. *Protoplasma* **222**, 13-21.

Calvert, P. D., Strissel, K. J., Schiesser, W. E., Pugh, E. N., Jr and Arshavsky, V. Y. (2006). Light-driven translocation of signaling proteins in vertebrate photoreceptors. *Trends Cell Biol.* **16**, 560-568.

Cooke, H. J. and Saunders, P. T. (2002). Mouse models of male infertility. *Nat. Rev. Genet.* **3**, 790-801.

Danshina, P. V., Geyer, C. B., Dai, Q., Goulding, E. H., Willis, W. D., Kitto, G. B., McCarrey, J. R., Eddy, E. M. and O'Brien, D. A. (2010). Phosphoglycerate kinase 2 (PGK2) is essential for sperm function and male fertility in mice. *Biol. Reprod.* **82**, 136-145.

Dantas, T. J., Daly, O. M. and Morrison, C. G. (2012). Such small hands: the roles of centrins/caltractins in the centriole and in genome maintenance. *Cell. Mol. Life Sci.* **69**, 2979-2997.

Davis, R. E., Swiderski, R. E., Rahmouni, K., Nishimura, D. Y., Mullins, R. F., Agassandian, K., Philp, A. R., Searby, C. C., Andrews, M. P., Thompson, S. et al. (2007). A knockin mouse model of the Bardet-Biedl syndrome 1 M390R mutation has cilia defects, ventriculomegaly, retinopathy, and obesity. *Proc. Natl. Acad. Sci. USA* **104**, 19422-19427.

Errabolu, R., Sanders, M. A. and Salisbury, J. L. (1994). Cloning of a cDNA encoding human centrin, an EF-hand protein of centrosomes and mitotic spindle poles. *J. Cell Sci.* **107**, 9-16.

Escalier, D. (2006). Knockout mouse models of sperm flagellum anomalies. *Hum. Reprod. Update* **12**, 449-461.

Fath, M. A., Mullins, R. F., Searby, C., Nishimura, D. Y., Wei, J., Rahmouni, K., Davis, R. E., Tayeh, M. K., Andrews, M., Yang, B. et al. (2005). Mkks-null mice have a phenotype resembling Bardet-Biedl syndrome. *Hum. Mol. Genet.* **14**, 1109-1118.

Fouquet, J. P., Kann, M. L., Combeau, C. and Melki, R. (1998). Gamma-tubulin during the differentiation of spermatozoa in various mammals and man. *Mol. Hum. Reprod.* **4**, 1122-1129.

Friedberg, F. (2006). Centrin isoforms in mammals. Relation to calmodulin. *Mol. Biol. Rep.* **33**, 243-252.

Gavet, O., Alvarez, C., Gaspar, P. and Bornens, M. (2003). Centrin4p, a novel mammalian centrin specifically expressed in ciliated cells. *Mol. Biol. Cell* **14**, 1818-1834.

Geimer, S. and Melkonian, M. (2005). Centrin scaffold in Chlamydomonas reinhardtii revealed by immunoelectron microscopy. *Eukaryot. Cell* **4**, 1253-1263.

Giessl, A., Pulvermüller, A., Trojan, P., Park, J. H., Choe, H. W., Ernst, O. P., Hofmann, K. P. and Wolfrum, U. (2004). Differential expression and interaction with the visual G-protein transducin of centrin isoforms in mammalian photoreceptor cells. *J. Biol. Chem.* **279**, 51472-51481.

Giessl, A., Trojan, P., Rausch, S., Pulvermüller, A. and Wolfrum, U. (2006). Centrins, gatekeepers for the light-dependent translocation of transducin through the photoreceptor cell connecting cilium. *Vision Res.* **46**, 4502-4509.

Harper, J. D., Sanders, M. A. and Salisbury, J. L. (1993). Phosphorylation of nuclear and flagellar basal apparatus proteins during flagellar regeneration in Chlamydomonas reinhardtii. *J. Cell Biol.* **122**, 877-886.

Hart, P. E., Glantz, J. N., Orth, J. D., Poynter, G. M. and Salisbury, J. L. (1999). Testis-specific murine centrin, Cetn1: genomic characterization and evidence for retroposition of a gene encoding a centrosome protein. *Genomics* **60**, 111-120.

Hart, P. E., Poynter, G. M., Whitehead, C. M., Orth, J. D., Glantz, J. N., Busby, R. C., Barrett, S. L. and Salisbury, J. L. (2001). Characterization of the X-linked murine centrin Cetn2 gene. *Gene* **264**, 205-213.

Hodges, M. E., Scheumann, N., Wickstead, B., Langdale, J. A. and Gull, K. (2010). Reconstructing the evolutionary history of the centriole from protein components. *J. Cell Sci.* **123**, 1407-1413.

Holzenberger, M., Lenzner, C., Leneuve, P., Zaoui, R., Hamard, G., Vaulont, S. and Bouc, Y. L. (2000). Cre-mediated germline mosaicism: a method allowing rapid generation of several alleles of a target gene. *Nucleic Acids Res.* **28**, E92.

Jiang, S. T., Chiou, Y. Y., Wang, E., Lin, H. K., Lee, S. P., Lu, H. Y., Wang, C. K., Tang, M. J. and Li, H. (2008). Targeted disruption of Nphp1 causes male infertility due to defects in the later steps of sperm morphogenesis in mice. *Hum. Mol. Genet.* **17**, 3368-3379.

Klein, U. R. and Nigg, E. A. (2009). SUMO-dependent regulation of centrin-2. *J. Cell Sci.* **122**, 3312-3321.

Koblenz, B., Schoppmeier, J., Grunow, A. and Lechtreck, K. F. (2003). Centrin deficiency in Chlamydomonas causes defects in basal body replication, segregation and maturation. *J. Cell Sci.* **116**, 2635-2646.

Laoukili, J., Perret, E., Middendorp, S., Houcine, O., Guennou, C., Marano, F., Bornens, M. and Tournier, F. (2000). Differential expression and cellular distribution of centrin isoforms during human ciliated cell differentiation in vitro. *J. Cell Sci.* **113**, 1355-1364.

Li, S., Chen, D., Sauve, Y., Mc Candles, J., Chen, Y. J. and Chen, C.-K. (2005). Rhodopsi-iCre transgenic mouse line for Cre-mediated rod-specific gene targeting. *Genesis* **41**, 73-80.

Manandhar, G., Sutovsky, P., Joshi, H. C., Stearns, T. and Schatten, G. (1998). Centrosome reduction during mouse spermiogenesis. *Dev. Biol.* **203**, 424-434.

McCarrey, J. R., Berg, W. M., Paragioudakis, S. J., Zhang, P. L., Dilworth, D. D., Arnold, B. L. and Rossi, J. J. (1992). Differential transcription of Pgk genes during spermatogenesis in the mouse. *Dev. Biol.* **154**, 160-168.

Middendorp, S., Paoletti, A., Schiebel, E. and Bornens, M. (1997). Identification of a new mammalian centrin gene, more closely related to Saccharomyces cerevisiae CDC31 gene. *Proc. Natl. Acad. Sci. USA* **94**, 9141-9146.

Middendorp, S., Küntziger, T., Abraham, Y., Holmes, S., Bordes, N., Paintrand, M., Paoletti, A. and Bornens, M. (2000). A role for centrin 3 in centrosome reproduction. *J. Cell Biol.* **148**, 405-416.

Mykytyn, K., Mullins, R. F., Andrews, M., Chiang, A. P., Swiderski, R. E., Yang, B., Braun, T., Casavant, T., Stone, E. M. and Sheffield, V. C. (2004). Bardet-Biedl syndrome type 4 (BBS4)-null mice implicate Bbs4 in flagella formation but not global cilia assembly. *Proc. Natl. Acad. Sci. USA* **101**, 8664-8669.

Nachury, M. V., Loktev, A. V., Zhang, Q., Westlake, C. J., Peränen, J., Merdes, A., Slusarski, D. C., Scheller, R. H., Bazan, J. F., Sheffield, V. C. et al. (2007). A core complex of BBS proteins cooperates with the GTPase Rab8 to promote ciliary membrane biogenesis. *Cell* **129**, 1201-1213.

Nishimura, D. Y., Fath, M., Mullins, R. F., Searby, C., Andrews, M., Davis, R., Andorf, J. L., Mykytyn, K., Swiderski, R. E., Yang, B. et al. (2004). Bbs2-null mice have neurosensory deficits, a defect in social dominance, and retinopathy associated with mislocalization of rhodopsin. *Proc. Natl. Acad. Sci. USA* **101**, 16588-16593.

Oakberg, E. F. (1956). Duration of spermatogenesis in the mouse and timing of stages of the cycle of the seminiferous epithelium. *Am. J. Anat.* **99**, 507-516.

Pulvermüller, A., Giessl, A., Heck, M., Wottrich, R., Schmitt, A., Ernst, O. P., Choe, H. W., Hofmann, K. P. and Wolfrum, U. (2002). Calcium-dependent assembly of centrin-G-protein complex in photoreceptor cells. *Mol. Cell. Biol.* **22**, 2194-2203.

Salisbury, J. L., Baron, A. T. and Sanders, M. A. (1988). The centrin-based cytoskeleton of Chlamydomonas reinhardtii: distribution in interphase and mitotic cells. *J. Cell Biol.* **107**, 635-641.

Salisbury, J. L., Suino, K. M., Busby, R. and Springett, M. (2002). Centrin-2 is required for centriole duplication in mammalian cells. *Curr. Biol.* **12**, 1287-1292.

Sanders, M. A. and Salisbury, J. L. (1989). Centrin-mediated microtubule severing during flagellar excision in Chlamydomonas reinhardtii. *J. Cell Biol.* **108**, 1751-1760.

Sedmak, T. and Wolfrum, U. (2011). Intraflagellar transport proteins in ciliogenesis of photoreceptor cells. *Biol. Cell* **103**, 449-466.

Sokolov, M., Lyubarsky, A. L., Strissel, K. J., Savchenko, A. B., Govardovskii, V. I., Pugh, E. N., Jr and Arshavsky, V. Y. (2002). Massive light-driven translocation of transducin between the two major compartments of rod cells: a novel mechanism of light adaptation. *Neuron* **34**, 95-106.

Taillon, B. E., Adler, S. A., Suhan, J. P. and Jarvik, J. W. (1992). Mutational analysis of centrin: an EF-hand protein associated with three distinct contractile fibers in the basal body apparatus of Chlamydomonas. *J. Cell Biol.* **119**, 1613-1624.

Tanaka, N., Goto, M., Kawasaki, A., Sasano, T., Eto, K., Nishi, R., Sugasawa, K., Abe, S. and Saitoh, H. (2010). An EF-hands protein, centrin-1, is an EGTA-sensitive SUMO-interacting protein in mouse testis. *Cell Biochem. Funct.* **28**, 604-612.

Trojan, P., Krauss, N., Choe, H. W., Giessl, A., Pulvermüller, A. and Wolfrum, U. (2008). Centrins in retinal photoreceptor cells: regulators in the connecting cilium. *Prog. Retin. Eye Res.* **27**, 237-259.

Turner, J. M. (2007). Meiotic sex chromosome inactivation. *Development* **134**, 1823-1831.

Wolfrum, U. and Salisbury, J. L. (1998). Expression of centrin isoforms in the mammalian retina. *Exp. Cell Res.* **242**, 10-17.

Wolfrum, U., Giessl, A. and Pulvermüller, A. (2002). Centrins, a novel group of Ca2+-binding proteins in vertebrate photoreceptor cells. *Adv. Exp. Med. Biol.* **514**, 155-178.

Won, J., Marín de Evsikova, C., Smith, R. S., Hicks, W. L., Edwards, M. M., Longo-Guess, C., Li, T., Naggert, J. K. and Nishina, P. M. (2011). NPHP4 is necessary for normal photoreceptor ribbon synapse maintenance and outer segment formation, and for sperm development. *Hum. Mol. Genet.* **20**, 482-496.

Wright, R. L., Salisbury, J. and Jarvik, J. W. (1985). A nucleus-basal body connector in Chlamydomonas reinhardtii that may function in basal body localization or segregation. *J. Cell Biol.* **101**, 1903-1912.

Zamboni, L. and Stefanini, M. (1971). The fine structure of the neck of mammalian spermatozoa. *Anat. Rec.* **169**, 155-172.

Zhang, Y. and He, C. Y. (2012). Centrins in unicellular organisms: functional diversity and specialization. *Protoplasma* **249**, 459-467.

Zhang, H., Li, S., Doan, T., Rieke, F., Detwiler, P. B., Frederick, J. M. and Baehr, W. (2007). Deletion of PrBP/delta impedes transport of GRK1 and PDE6 catalytic subunits to photoreceptor outer segments. *Proc. Natl. Acad. Sci. USA* **104**, 8857-8862.

Zhang, H., Fan, J., Li, S., Karan, S., Rohrer, B., Palczewski, K., Frederick, J. M., Crouch, R. K. and Baehr, W. (2008). Trafficking of membrane-associated proteins to cone photoreceptor outer segments requires the chromophore 11-cis-retinal. *J. Neurosci.* **28**, 4008-4014.

Germline deletion of *Cetn1* causes infertility in male mice

Prachee Avasthi[1,*,#], Jan Frederik Scheel[2,*], Guoxin Ying[1], Jeanne M. Frederick[1], Wolfgang Baehr[1,3,4], Uwe Wolfrum[2]

Supplemental figures and tables

Figure S1.

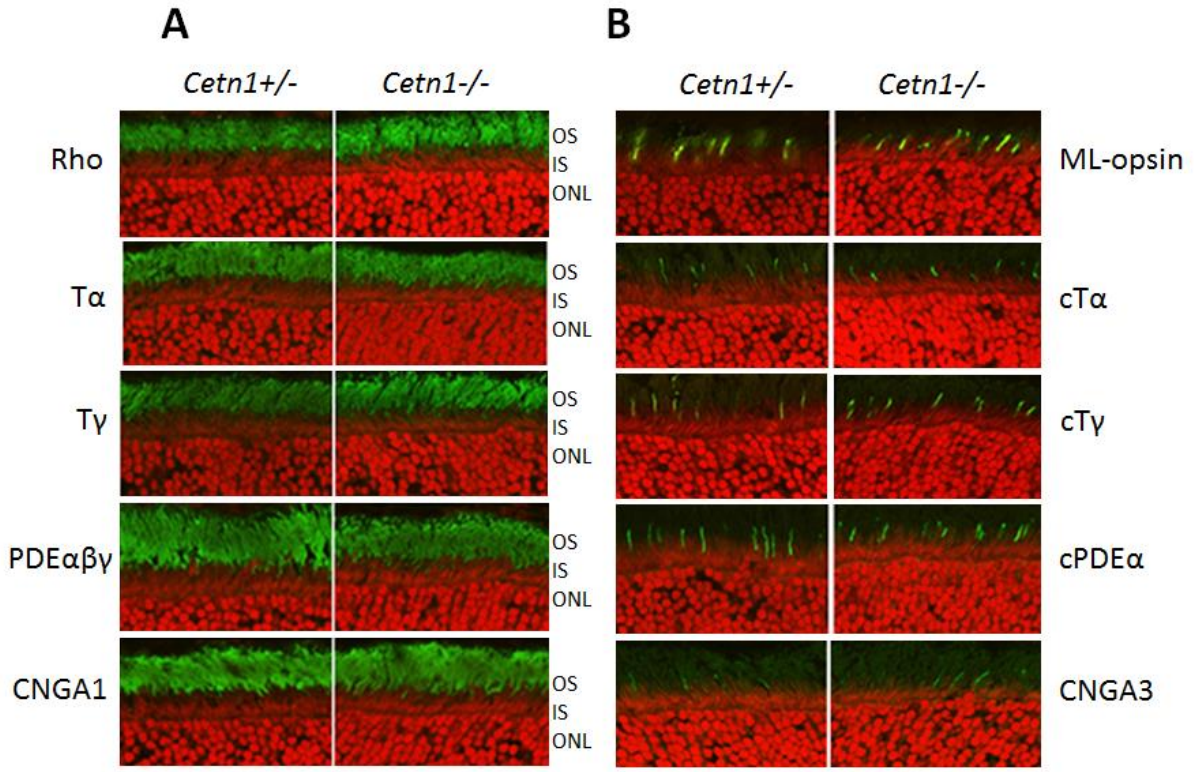

Figure S1. Immunolocalization of phototransduction proteins in retinas of *Cetn1*$^{+/-}$ and *Cetn1*$^{-/-}$ mice. **A** (left vertical panel), localization of rhodopsin, transducin subunits, PDEαβγ, and CNGA1 in rod outer segments. **B** (right vertical panel), distribution of ML-opsin, cone transducin (cTα), cone PDEα, and CNGA3 in cone outer segments. Heterozygote retinas, indistinguishable from wild-type, were used as reference. Sections of heterozygote (left) and homozygous knockout (right) retinas were immunolabeled using antibodies directed against the indicated target antigens (green) and contrasted with propidium iodide (red). Antibodies used to detect rod- and cone-specific antigens have been described (Avasthi et al., 2009; Baehr et al., 2007; Zhang et al., 2008). No obvious difference in localizations was observed between genotypes. OS, outer segments; IS, inner segments; ONL, outer nuclear layer.

Figure S2.

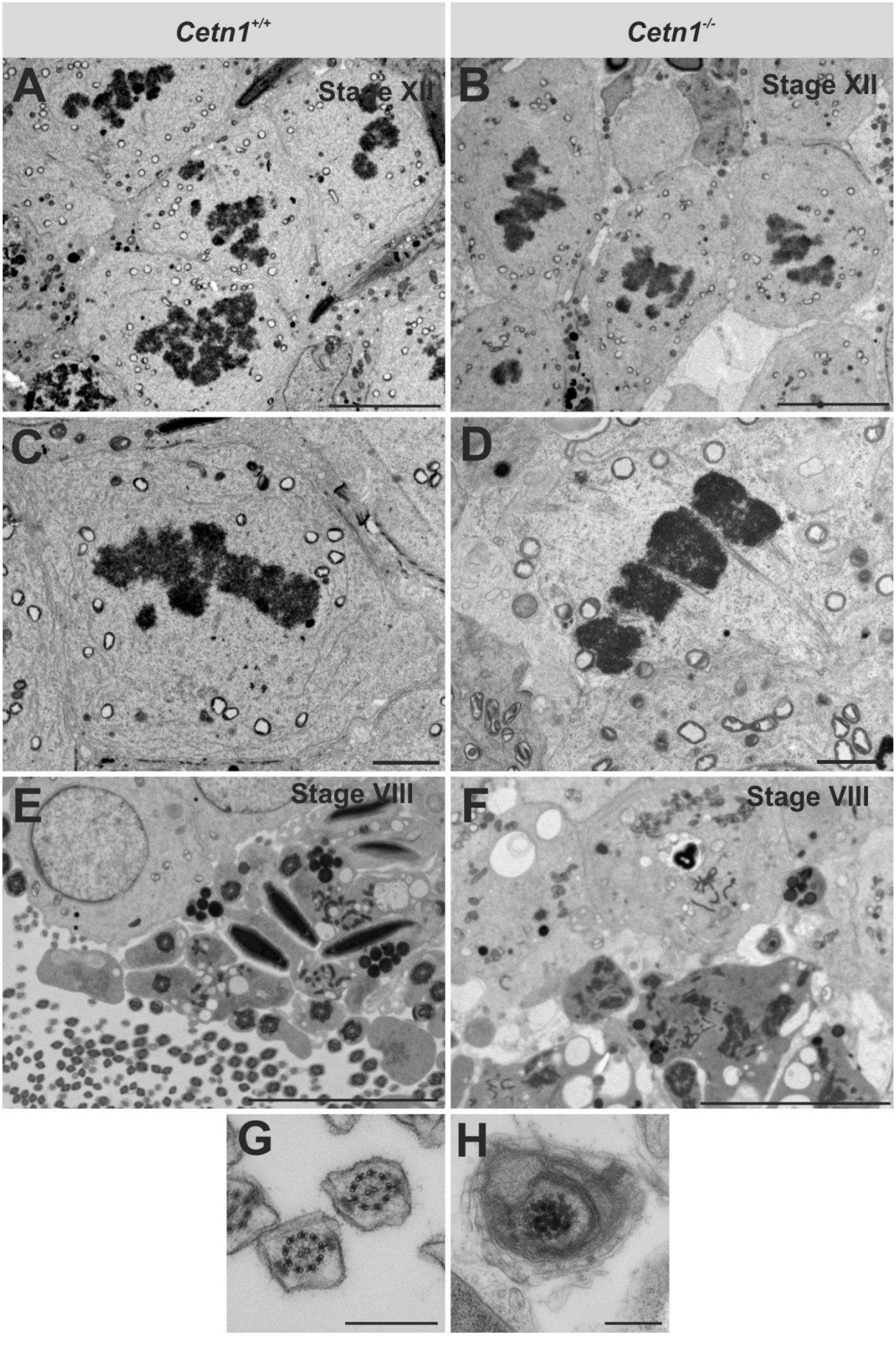
Cetn1+/+
Cetn1-/-
A
Stage XII
B
Stage XII
C
D
E
Stage VIII
F
Stage VIII
G
H

Figure S2. Electron microscope analysis of seminifereous tubules of Cetn1$^{+/+}$ and Cetn1$^{-/-}$ mice. A, B spermatocytes during meiosis of stage XII seminiferous tubules. Normal condensation and chromosome pairing is evident in spermatocytes of *Cetn1*$^{-/-}$ seminiferous tubules. **C, D** higher magnifications of spermatocytes in metaphase. Chromosomes are equatorially arranged in Cetn1$^{+/+}$ and Cetn1$^{-/-}$. The arrangement of spindle microtubules in *Cetn1*$^{-/-}$ appeared normal. **E, F** 2nd generation spermatids directly prior to spermiation at stage VIII in *Cetn1*$^{+/+}$ and *Cetn1*$^{-/-}$ seminiferous tubules. In E, elongated and mature spermatid heads are found facing the tubule lumen and additionally, several spermatid flagella are observed in cross section. In F, electron-dense material is present instead of mature spermatids. **G,** cross section through a *Cetn1*$^{+/+}$ flagellum showing the characteristic axonemal microtubule 9x2+2 arrangement and side fibers. **H,** cross section through the sole *Cetn1*$^{-/-}$ flagellum found, revealing severe disorganization of axonemal microtubules. **Bars: A, B, E, F: 5 µm, C, D: 1 µm, G, H: 0.5 µm.**

Figure S3.

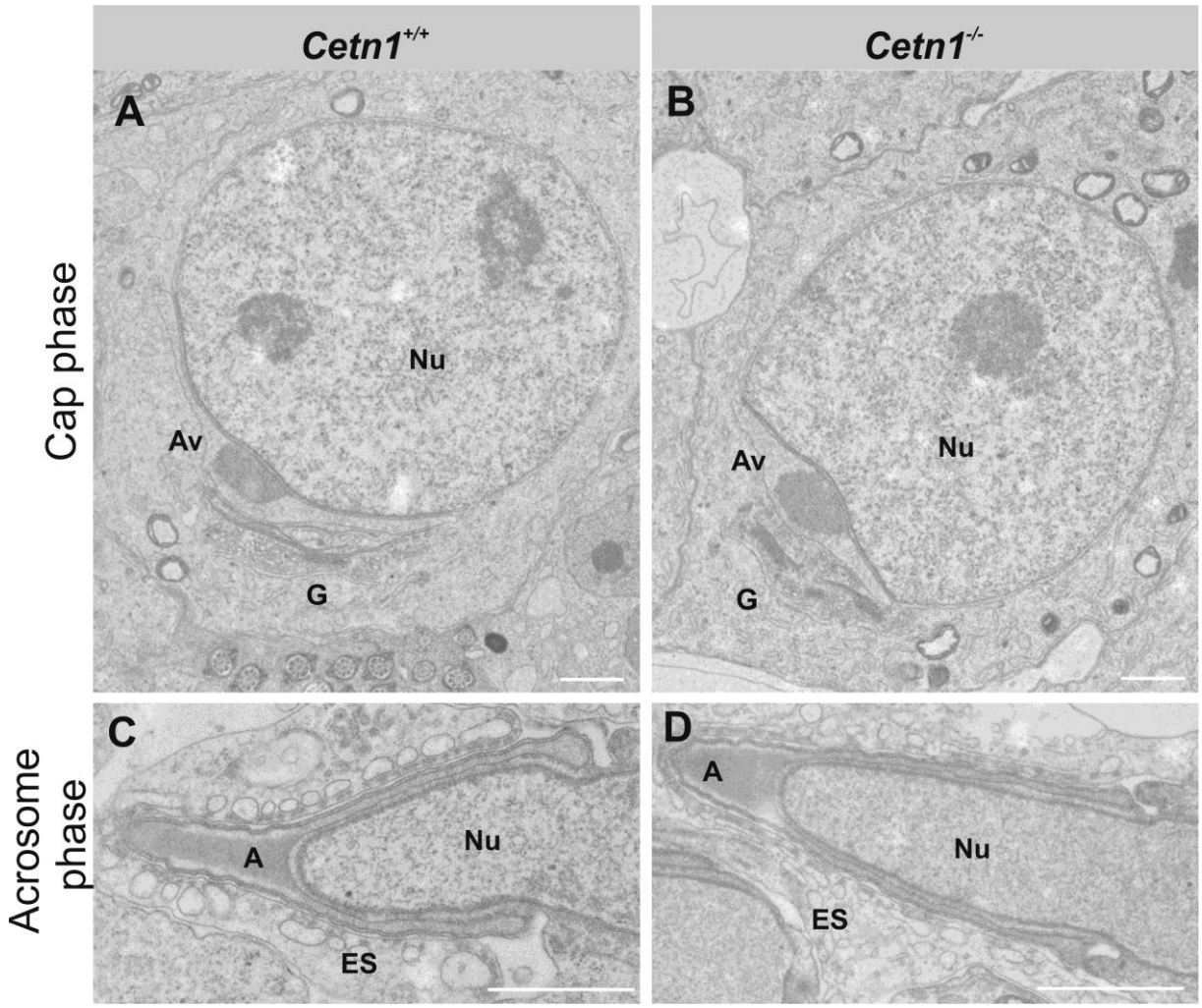

Figure S3. Transmission electron micrographs of early-stage spermiogenesis from *Cetn1*$^{+/+}$ and *Cetn1*$^{-/-}$ mice. A, B cap phase spermatids from *Cetn1*$^{+/+}$ and *Cetn1*$^{-/-}$ mice, and **C, D** acrosome phase spermatids display no difference in ultrastructure. **Av:** acrosomic vesicle, **G:** Golgi apparatus, **Nu:** nucleus, **A:** acrosome, **ES:** ectoplasmic specialization. **Bars: 1 µm.**

Figure S4.

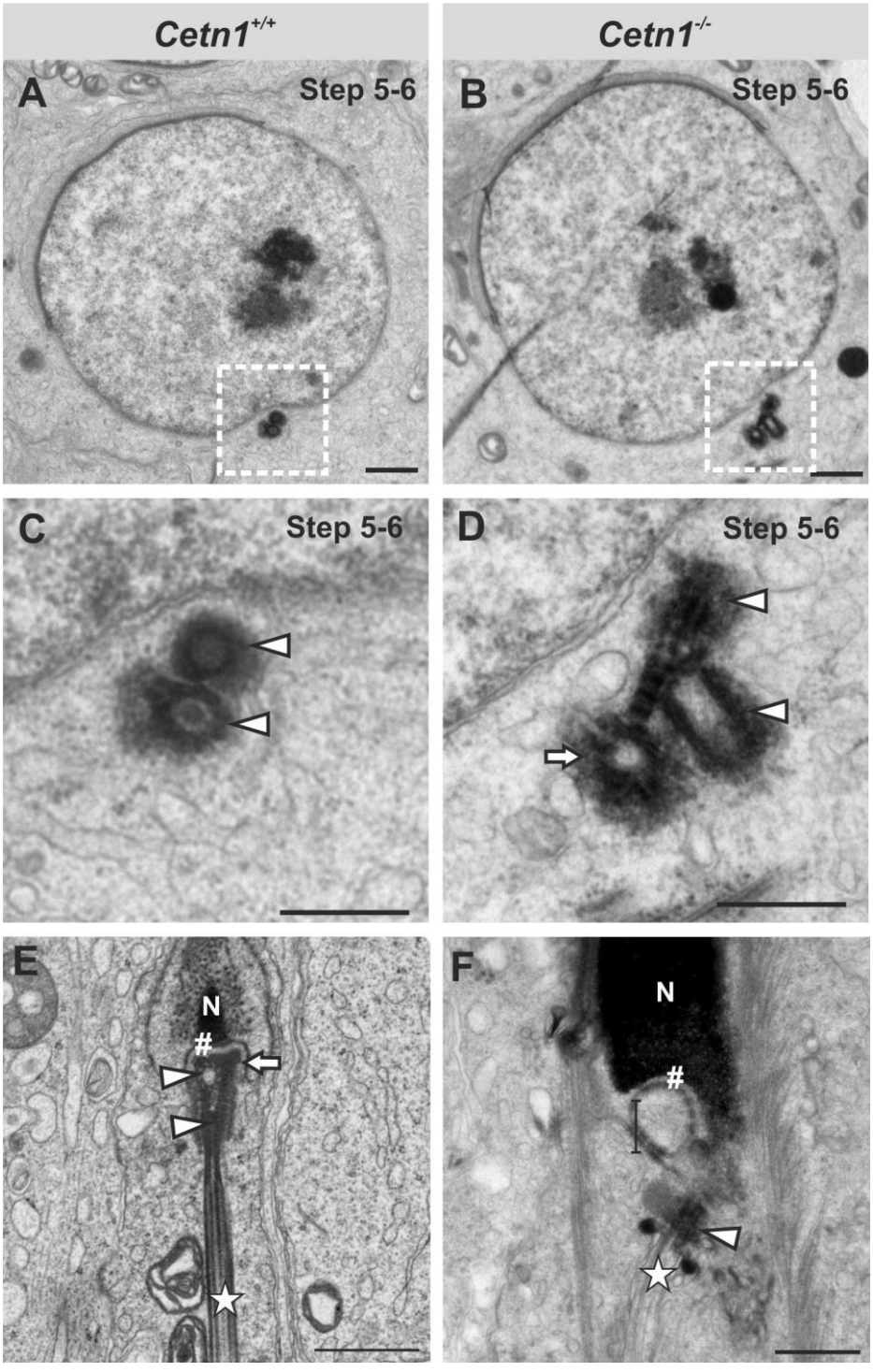

Figure S4. Electron microscopy of spermatid centrioles. **A, B,** round post-meiotic spermatids in step 5-6 of *Cetn1*$^{+/+}$ and *Cetn1*$^{-/-}$ testes. Centrioles of the centrosome/basal body complex are located within the perinuclear compartment. **C, D,** higher magnification taken from A and B. No abnormalities were detectable in *Cetn1*$^{-/-}$ spermatid centrioles (**arrowheads**); adjunct (**arrow**) formation was initiated and centriole sizes were of normal proportions (see text). **E,F,** mature spermatids in step 15. **E,** fully-developed striated body (**arrowhead**) of a *Cetn1*$^{+/+}$ mouse spermatid embedded in the nuclear fossa (**#**) of the nucleus (**N**). The sperm flagella axoneme (**star**) exhibited a dense structure with straight projection from the striated body. **F,** The centriolar complex (**arrowhead**), observed rarely in mature *Cetn1*$^{-/-}$ spermatids, lacks a striated body. The axoneme (**star**), nuclear fossa (**#**) and basal body (**arrowhead**) each exhibit unstable, atypical structure. **Bars: A, B: 1 µm, C - F: 0.5 µm.**

Figure S5.

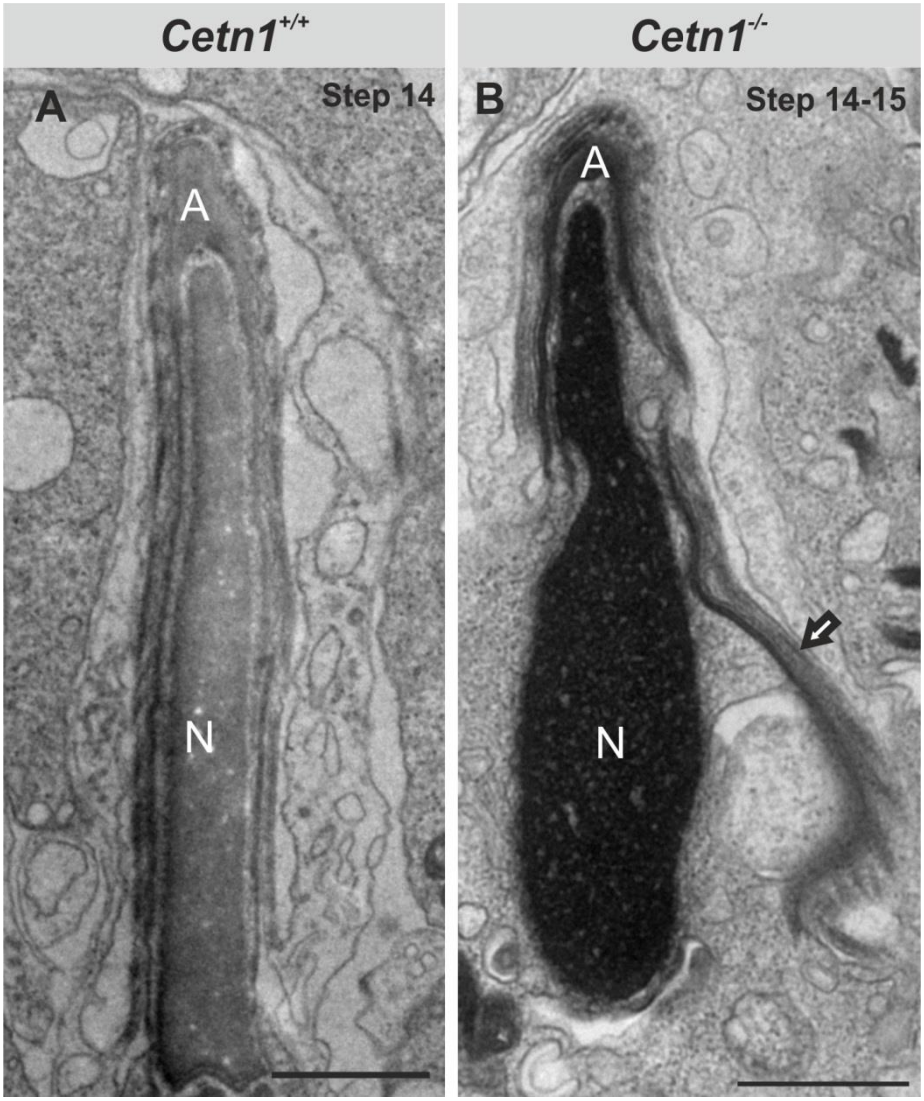

Figure S5. Ultrastructure of step 14-15 spermatids. A, *Cetn1*$^{+/+}$ spermatid at step 14 with normal acrosome **(A)** and nucleus **(N)** morphology. **B**, *Cetn1*$^{-/-}$ spermatid at step 14-15 displays severe defects in membrane systems. The acrosome **(A)** disintegrates and dissolves **(arrow)** from the electron-dense spermatid nucleus **(N)**. **Bars: 0.5 µm.**

Figure S6.

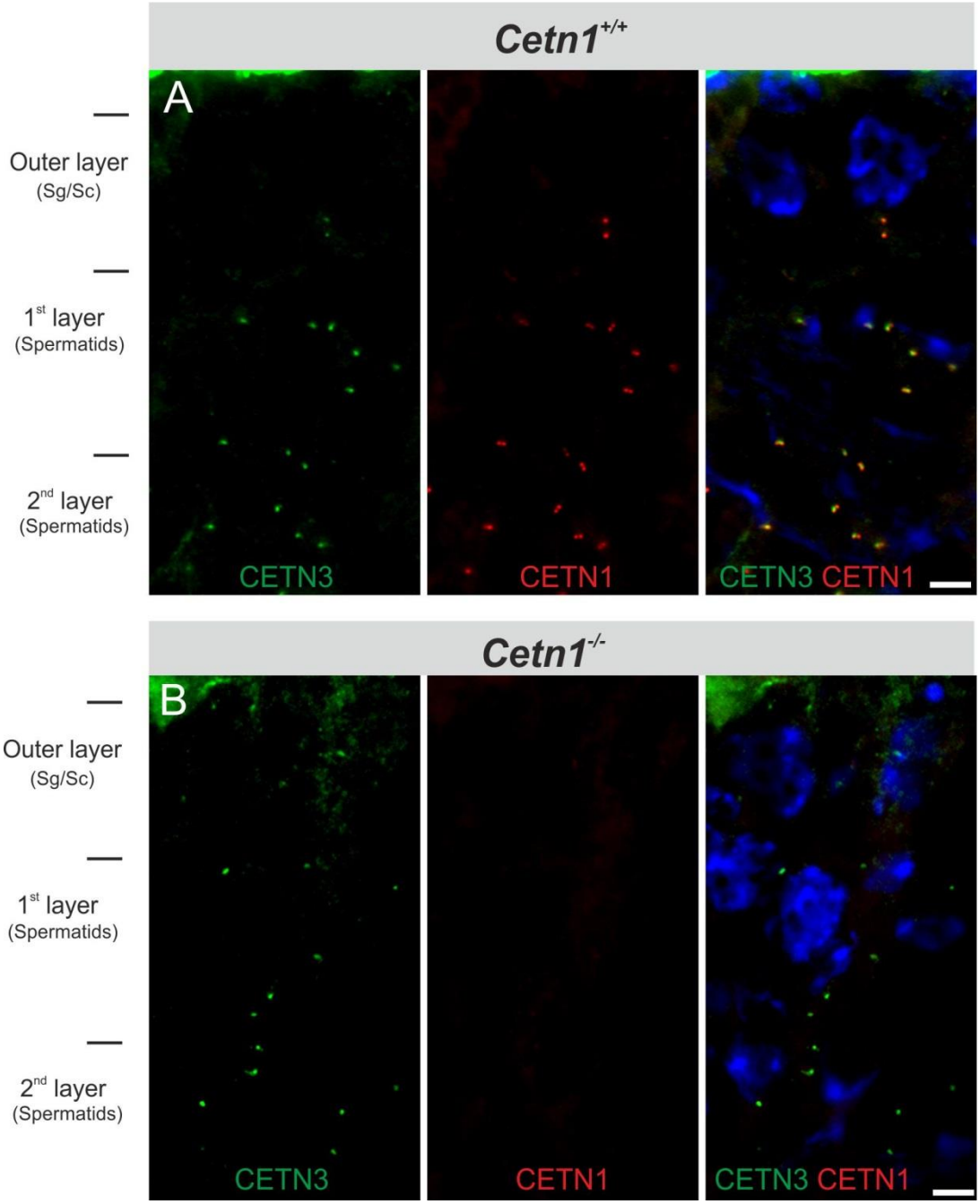

Figure S6. CETN1 and CETN3 immunolabeling of seminifereous tubules from *Cetn1*$^{+/+}$ and *Cetn1*$^{-/-}$ mice. A Antibodies directed against CETN1 (red) and CETN3 (green) label centrioles (fluorescent dots) in all layers and germ cell types of *Cetn1*$^{+/+}$ seminifereous tubules. **B** CETN3 labeling was present in all germ cell types, while CETN1 was undetectable in *Cetn1*$^{-/-}$ mice. DAPI (blue) staining of nuclei. **Sg:** spermatogonia; **Sc:** spermatocytes. **Bars: 5 µm.**

Figure S7.

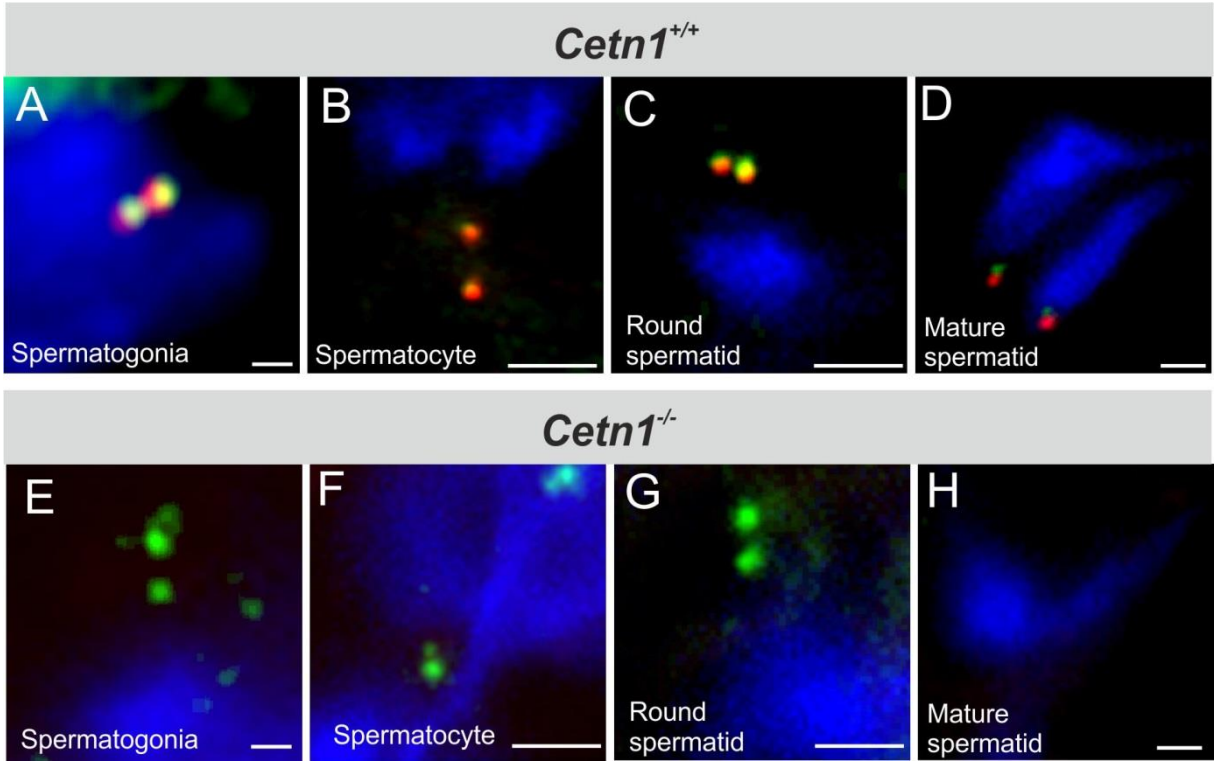

Figure S7. CETN1 (red) and CETN3 (green) immunolabeling of spermatogonia (A, E), spermatocytes (B, F), round spermatids (C, G) and mature spermatids (D, I) of seminifereous tubules from *Cetn1*$^{+/+}$ and *Cetn1*$^{-/-}$ mice. No obvious difference of CETN3 labeling was discerned between *Cetn1*$^{+/+}$ and *Cetn1*$^{-/-}$ spermatogonia, spermatocytes and early round spermatids. By contrast, sperm heads (DAPI, blue) of *Cetn1*$^{-/-}$ mature spermatids (**H**) were "bent" with centrioles displaying no immunoreactivity for CETN3 as well as CETN1. **Bars: 1 µm**.

Supplemental Table

Table S1: *Cetn1* mice body weights, testis weights, sperm number and deformed sperm among genotypes.

Genotype	Body weight (g)	Testis weight (mg)	Amount of sperm (%)	% sperm deformed
***Cetn1*$^{+/+}$**	31.6 ±2.5	93 ±6	100%	1.5% ±0.2
***Cetn1*$^{+/-}$**	30.9 ±2.7	92 ±3	100% ±1.8	1.7% ±0.4
***Cetn1*$^{-/-}$**	32.1 ±2.1	94 ±4	1.1% ±0.2	100%

Male mice from 6 litters were analyzed (N=24, consisting of five *Cetn1*$^{+/+}$, eleven *Cetn1*$^{+/-}$ and eight *Cetn1*$^{-/-}$). No abnormality of body or testis weight was measurable. Average total sperm count of *Cetn1*$^{+/+}$ mice was set to 100%; no difference in *Cetn1*$^{+/-}$ sperm count was found. *Cetn1*$^{-/-}$ sperm number was reduced drastically to 1.1% ±0.2, with 100% of these exhibiting deformation.

Table S2: Quantification of the number of germ cell types in seminifereous tubuli of Cetn $^{+/+}$ and Cetn1$^{-/-}$ mice.

Genotype	No. spermatogonia	No. spermatocytes	No. spermatids	Epithelial thickness (µm)
***Cetn1*$^{+/+}$**	3.0 ±1.4	4.4 ±1.1	16.2 ±6.8	92.1 ±3.2
***Cetn1*$^{-/-}$**	3.2 ±0.8	3.8 ±1.2	16.8 ±5.0	91.0 ±3.2

Quantification of the numbers of germ cell types from *Cetn1*$^{+/+}$ and *Cetn1*$^{-/-}$ seminifereous tubuli (N=5). Germ cells of *Cetn1*$^{+/+}$ and *Cetn1*$^{-/-}$ tubuli seminiferi at stage IX of spermatogenesis were counted in the area of a rectangle 100 µm x 50 µm. No significant difference in average values was detected for *Cetn1*$^{-/-}$ germ cells.